Atmospheric Research 197 (2017) 211–223

Contents lists available at ScienceDirect

Atmospheric Research

journal homepage: www.elsevier.com/locate/atmosres

Internally mixed black carbon in the Indo-Gangetic Plain and its effect on absorption enhancement

Navaneeth M. Thamban[a], S.N. Tripathi[a,b,*], Shamjad P. Moosakutty[a], Pavan Kuntamukkala[a], V.P. Kanawade[c]

[a] Department of Civil Engineering, Indian Institute of Technology, Kanpur, India
[b] Centre for Environmental Science and Engineering, Indian Institute of Technology, Kanpur, India
[c] University Centre for Earth & Space Sciences, University of Hyderabad, India

ARTICLE INFO

Keywords:
Black carbon
Indo-Gangetic Plain
Mixing state
Absorption enhancement
Organics
Inorganics

ABSTRACT

We present the systematic analysis of individual black carbon (BC) mixing state and its impact on radiative forcing from an urban Indian city, Kanpur, located in Indo-Gangetic Plain (IGP). Simultaneous measurements using Single Particle Soot Photometer (SP2), Photo-Acoustic Soot Spectrometer (PASS-3) and High-Resolution Time-of-Flight Aerosol Mass Spectrometer (AMS) were conducted from 8 January 2015 to 28 February 2015 at Kanpur. BC mass and number concentrations varied between 0.7 and 17 μg/m^3 and 277–5866 #/cm^3 with a mean of 4.06 μg/m^3 and 1314 #/cm^3, respectively. The diurnal variation of BC mass concentration showed a traffic hour peak during both the morning and late night. The mean fraction of "thickly coated BC" particles (fTC_{BC}) was found to be 61.6%, indicating that a large fraction of BC particles was internally mixed. The fTC_{BC} increased after sunrise with a peak at about noontime, indicating that the formation of secondary organic aerosol under active photochemistry can enhance organic coating on a core of black carbon. High-resolution positive matrix factorization (HR-PMF) factors showed distinct characteristics with fTC_{BC}. While primary organic aerosols like cooking organic aerosols (COA) and biomass burning organic aerosols (BBOA) were negatively correlated with fTC_{BC} ($r = -0.78$ and -0.51, respectively), aged low volatile oxygenated organic aerosol (LVOOA) was forming a coating over BC ($r = 0.6$). Similar positive correlation of fTC_{BC} with inorganic species like ammonium ($r = 0.58$) and nitrate ($r = 0.47$) further suggested that BC appears to be largely coated with LVOOA, ammonium, and nitrate. A positive correlation between the fTC_{BC} and the mass absorption cross-section at 781 nm (MAC_{781}) was also observed ($r = 0.58$). Our results suggest that the observed fTC_{BC} could amplify the MAC_{781} approximately by a factor of 1.8, which may catalyze the positive radiative forcing in the IGP.

1. Introduction

Black carbon (BC) is emitted into the atmosphere by incomplete combustion of fossil fuels and biomass burning (Bond et al., 2013; Chen et al., 2015; Novakov et al., 2000; Oshima et al., 2009; Talukdar et al., 2015; Tiwari et al., 2016; Vaishya et al., 2017; Verma et al., 2017). In spite of its short atmospheric lifetime of about 4 to 12 days (Cape et al., 2012; Schwarz et al., 2006), it plays an important role in radiative forcing (Jacobson, 2001) by strongly absorbing solar radiation and lowering the fraction of the extinction due to scattering (Penner et al., 1998; Ram et al., 2012b; Ramanathan et al., 2001). While BC aerosols are generally externally mixed and hydrophobic when they are freshly emitted (Willis et al., 2016; Zhang et al., 2016), atmospheric aging leads to internally mixed BC with hydrophilic compounds (e.g. organic acids and ammonium sulfate) (Zhang et al., 2015) through condensation and coagulation which increases its hygroscopicity and size (Liu et al., 2010; Moteki et al., 2007). These hydrophilic internally mixed BC can act as condensation nuclei (CCN) (McMeeking et al., 2011a; Shiraiwa et al., 2007) which can affect the climate (Cappa et al., 2012) by changing its wet scavenging efficiency and atmospheric lifetime (Oshima et al., 2009).

Kanpur is an industrial city located in the Indo-Gangetic Plain (IGP) which is one of the most populated and polluted regions in northern India (Ram et al., 2010). While the BC concentration in Kanpur is found to be comparable to other developing nations like China, it is much higher than that of developed nations like Europe and United States (Ramachandran and Rajesh, 2007; Tripathi et al., 2005a). BC concentrations in Kanpur reach significantly high levels (17 μg/m^3) in winter period, perhaps due to the combined effect of the shallow boundary layer height (Baxla, 2009; Tripathi et al.,2007) and increased

* Corresponding author at: Department of Civil Engineering, Indian Institute of Technology, Kanpur, India.
E-mail address: snt@iitk.ac.in (S.N. Tripathi).

http://dx.doi.org/10.1016/j.atmosres.2017.07.007
Received 22 March 2017; Received in revised form 4 July 2017; Accepted 10 July 2017
Available online 12 July 2017
0169-8095/

anthropogenic emissions (biomass/trash burning) (Kanawade et al., 2014; Nair et al., 2007). These anthropogenic emissions also generate hygroscopic organic and inorganic aerosols along with BC. Furthermore, the high relative humidity (RH) in winter period promotes the internal mixing of these hygroscopic aerosols with BC, where they assume to form a core-shell structure with a BC core (Bond and Bergstrom, 2006). Previous studies indicate that the coating of these non-absorbing organic and inorganic aerosols on BC can enhance the magnitude of solar radiation absorption and this is generally termed as the lensing effect (Liu et al., 2015; Schwarz et al., 2008; Shamjad et al., 2012). This enhancement in absorption depends upon the type of coating material, the thickness of the coating on BC and the morphology of BC (Andreae and Gelencsér, 2006; Laborde et al., 2013; Liu et al., 2015).

Most of the previous studies in IGP used photoacoustic techniques, filter-based measurements, modelled algorithms and thermal optical measurements to measure the BC mass and its mixing state (Dey et al., 2008; Kaul et al., 2011; Raju et al., 2016; Ram et al., 2016; Shamjad et al., 2015, 2012; Tripathi et al., 2005b). But traditional filter based BC measurements (e.g. Aethalometer) are prone to limitations which overestimate the light absorption due to multiple scattering substrates (Arnott et al., 2005), whereas at higher RH photo-acoustic methods underestimate absorption and affect the indirect estimation of BC (Arnott, 2003). Moreover, these bulk techniques cannot provide the information on mixing state of individual BC particles (Li et al., 2016) which is very important in the BC radiative forcing calculation as the internally mixed BC particles can increase the positive radiative forcing (Jacobson, 2001).

Studies also tried to depict mixing state and morphology of BC using single particle offline measurements using electron and X-ray microscopy. (China et al., 2013) identified that the biomass burning generates BC with varying morphologies and 50% of soot particles were embedded (heavily coated). In another study, (Adachi et al., 2014) found that 75% of BC was internally mixed with sulfate in Japan. Generally, BC was more internally mixed with sulfate and organics (Adachi and Buseck, 2008; Fu et al., 2012), spherical in shape once it is thickly coated (Ueda et al., 2016) and condensation of organics and inorganics over BC showed an increase in its particle size (Moffet et al., 2016).

The present study used the Droplet Measurement Technologies (DMT) Single Particle Soot Photometer (SP2), which has gained more attention in recent years because of its higher selectivity and specificity towards refractory BC measurement. BC measurements using SP2 are also free from most of the artifacts of the aforesaid previously used instruments. Here, we report the mixing state of individual BC particles at an urban site, Kanpur, in IGP during the winter of 2014–2015. Alongside SP2 measurements, optical properties of BC and non-refractory submicron concentration of aerosols were also measured simultaneously using the DMT Photo Acoustic Soot Spectrometer (PASS-3) and Aerodyne High-Resolution Time-of-Flight Aerosol Mass Spectrometer (HR-ToF-AMS, hereafter referred to as AMS), respectively.

2. Experimental methods

2.1. Sampling site

Measurements were carried out at the Centre for Environmental Science and Engineering (CESE) building in the Indian Institute of Technology, Kanpur campus (26.46°N, 80.32°E, 142 m above mean sea level) from 8 January 2015 to 28 February 2015, characterized as winter season. Kanpur is an industrial hub of northern India, which is located in the central part of IGP where coal-based power plants, fossil fuel combustion, and biomass burning significantly contribute towards the total anthropogenic aerosol loading (Kanawade et al., 2014; Ram et al., 2010) and absorbing aerosols. Specifically, the winter season in northern India is characterized by the widespread biomass/trash burning, resulting in a high aerosol loading due to prevailing stable weather conditions (Dey et al., 2005; Singh et al., 2004) and also witnesses frequent occurrence of fog with high RH conditions (Kaul et al., 2011).

A high mass concentration of absorbing aerosols (Sanap and Pandithurai, 2015) and organics (Chakraborty et al., 2015), shallow boundary layer height (Nair et al., 2007) and frequent fog episodes (Kaul et al., 2011; Ram et al., 2012a) in the winter period mark IGP as one of the regional BC hotspot and an ideal location to study aerosols mixing state (Bhattu and Tripathi, 2015; Ram et al., 2014). These complex ambient characteristics and high aerosol loading can further interact with the climatology of downwind receptor sites. To understand the significance of BC loading in IGP to the downwind receptor sites, Hybrid Single-Particle Lagrangian Integrated Trajectory (HYSPLIT 4) (Draxler et al., 2016) model forward trajectory analysis was performed for air mass originating from our site. The data was retrieved from Global Data Assimilation System (GDAS) and the model was run at the height of 50 m above ground at an interval of 5 days (starting at "6:30 UTC") from January 10 to February 25. The air mass forward trajectories show (Fig. 1) that the mixing state of BC in IGP can influence the radiative forcing calculation of both short range (east and south-east India) and also long range (Tibetan plateau and China) receptor sites.

2.2. Instrumentation

SP2, PASS-3, and AMS all were kept inside an air-conditioned laboratory with sampling lines extended towards the open atmosphere. These instruments were operated in parallel to analyze the real-time characteristics of BC and non-refractory organics and inorganics simultaneously. Ambient aerosols were dried by using a silica diffusion dryers to effectively reduce the RH to < 10% before passing to AMS and PASS-3. SP2, which can operate between an RH of 0–100%, was directly connected to the ambient air similar to the setup discussed elsewhere (Laborde et al., 2012; Liu et al., 2013; Shamjad et al., 2016).

2.2.1. Single Particle Soot Photometer (SP2)

SP2 was used to measure mass, number concentration and size distribution of BC particles. In SP2, an intracavity Nd: YAG laser beam of 1064 nm was used to quantify the mass of individual BC particles. The TEM00 mode laser beam intercepts the aerosol flow (which was taken as 30 Volumetric Cubic Centimeter per Minute (VCCM) for the present study) in a perpendicular plane. The Nd: YAG laser beam heats up the black carbon particle to its vaporization temperature. The emitted incandescent light was detected using avalanche photodiodes (Moteki and Kondo, 2010, 2007; Schwarz et al., 2006; Stephens et al.,

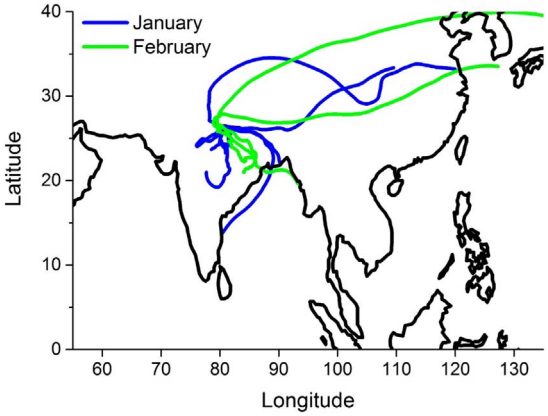

Fig. 1. HYSPLIT 5-day forward trajectory of air mass from January to February. The model was run at 50 m above from ground from January 10 to February 25 at an interval of 5 days, starting at "6:30 UTC".

2003; Subramanian et al., 2010; Wang et al., 2014a). The magnitude of the elastically scattering signal indicates the optical diameter of the particle (Stephens et al., 2003). Principle and operating details of SP2 were explained in other studies in detail (Gao et al., 2007; Moteki and Kondo, 2007; Schwarz et al., 2010, 2006; Stephens et al., 2003). While earlier SP2 studies assumed that incandescent signal directly indicates the mass of refractory BC irrespective of the mixing state or morphology (Slowik et al., 2007), recent studies found that SP2 measurements are prone to limitations. (Sedlacek et al., 2015) identified that the SP2 operating conditions, particle morphology, fragmentation of BC cores which are coated very thickly, and the location of BC core in core-shell structure plays an important role in governing the signals and SP2 behavior.

SP2 can also be used to estimate the mixing state of BC. The heating up of internally mixed BC particles in the laser beam of SP2 will cause the non-refractory coating to evaporate first and to produce a scattering signal peak before the BC core incandescent signal reaches its peak value. The time delay (ΔT, in μs) between this scattering and incandescent signal peak is traditionally used to characterize between thinly coated and thickly coated BC particles and is generally called the time lag approach (Moteki and Kondo, 2007; Shiraiwa et al., 2007; Subramanian et al., 2010; Wang et al., 2014a). The fraction of "thickly coated BC" particles (fTC_{BC}) is the ratio of the number of thickly coated BC particles to the sum of thinly coated particles and thickly coated BC particles (Sedlacek et al., 2012). The present study found that the threshold time lag (the minimum observed value in the bimodal frequency distribution of lag time) of 2 μs was separating the thinly coated BC particle ($\Delta T < 2$ μs) and thickly coated BC particles ($\Delta T > 2$ μs) similar to a previous study (Moteki et al., 2007).

2.2.2. Photo Acoustic Soot Spectrometer (PASS-3)

A three wavelength PASS-3 was used to measure the light scattering and absorption coefficients in Mm^{-1} simultaneously in an acoustic resonator cavity. The aerosol gets heated up by absorbing incoming laser radiation. The expansion of aerosol-laden air due to the heated aerosol creates a pressure disturbance. The acoustic wave resulting from the pressure disturbance was measured by the microphone (Arnott et al., 1999).

PASS-3 was calibrated for scattering and absorption coefficients following the standard procedure given elsewhere (Arnott et al., 2000; Nakayama et al., 2015). First, scattering coefficient was calibrated using a high concentration of polydisperse ammonium sulfate $(NH_4)_2SO_4$ particles. The acquired scattering coefficients ($b_{sca}(\lambda)$) were compared with the extinction coefficients calculated using Beer-Lambert law by identifying the changes in light intensity that traverse the acoustic cell in the absence and presence of particles (Nakayama et al., 2015). Even though many studies used NO_2 gas for absorption calibration (Arnott et al., 2000; Nakayama et al., 2014; Ueda et al., 2016), the present study calibrated the absorption coefficient (B_{abs}) measurements of PASS-3 using kerosene flame soot (Arnott et al., 2000) due to the unavailability of NO_2 gas. The generated soot from kerosene flame was maintained at relative steady concentration using a mixing chamber (30 cm * 30 cm * 30 cm) to measure the corresponding extinction and absorption of the kerosene generated soot. The extinction coefficients of these absorbing aerosols were identified using Beer-Lambert law. The absorption calibration factors were identified by plotting B_{ext}-B_{scat} versus B_{abs} for three distinct wavelengths of PASS-3.

PASS-3 was operated with an aerosol flow rate of 1 l per minute (lpm) and a data collection frequency of 0.5 Hz (Lan et al., 2013; Shamjad et al., 2015). Scattering information from PASS-3 is not reported as it is not well within the objective of the present study. Here, we only report the results from a single wavelength (781 nm) of PASS-3. Absorption information of PASS-3 at 532 nm is discarded due to low laser power and absorption information at 405 nm is not reported in the present manuscript as it shows very weak correlation ($r = 0.1$) with fTC_{BC}. This weak correlation between fTC_{BC} and absorption at 405 nm can be due to the absorption contribution from externally mixed brown carbon (Liu et al., 2015; Shamjad et al., 2016). The aerosol stream was dried to an RH of < 10% before passing to PASS-3 as higher RH can affect the photoacoustic measurement and indirect estimation of BC (Arnott, 2003).

2.2.3. High-Resolution Time-of-Flight Aerosol Mass Spectrometer (AMS)

Aerodyne AMS was used to measure mass concentration and size distribution of non-refractory materials of diameter below 1 μm (DeCarlo et al., 2006). In AMS, non-refractory species are heated up to a vaporization temperature of ~600 °C and followed by electrical ionization at approximately 70 eV. AMS measures the mass concentration of inorganics (ammonium, nitrate, sulfate and chloride) and OA. The AMS measurements from the V-mode data were further processed to calculate mass concentration of non-refractory organics and inorganics. V-mode is a mode of operation of HR-ToF-AMS where ions follow a standard reflection pattern. In V-mode, ions follow a trajectory from the extraction region to reflectron and back to multichannel plate (MCP) detector. The effective path length of V-mode is 1.3 m (DeCarlo et al., 2006). Particle time of flight (PToF) data was used to identify the size distributions of aforesaid species in this study.

Standard ionization efficiency (IE) and particle time of flight (PToF) calibrations were performed on AMS according to previously reported studies (Jayne et al., 2000; Jimenez et al., 2003). IE calibrations were performed before, during and after the experiments. Average relative ionization efficiency (RIE) for organics for the sampling period was assumed to be 1.4 while the calculated average RIE for NH^+ was 4.6. The PToF calibration was performed on size selected ammonium sulfate particles with the help of differential mobility analyzer (DMA 3081, TSI).

2.3. Data analysis

The data from the SP2 was analyzed using standard SP2 software version 4.3.3. The time lag information, number concentration of BC was further processed to hourly values for data analysis. Incandescent signals of SP2 were calibrated with Aquadag® as BC calibration material. Even though Aquadag cannot exactly mimic the ambient BC characteristics (Laborde et al., 2012; Moteki and Kondo, 2010), it is traditionally used as a proxy for EC (Gong et al., 2016; Zhang et al., 2016). Differential mobility analyzer (DMA, TSI) was used to generate size selected Aquadag at particular mobility diameter (80–620 nm) which then passed to SP2 to analyze the signals. Corresponding masses of BC were noted at high gain and low gain detectors (Fig. S3) of SP2 by using an effective density of BC i.e.1800 kg/m^3 (Bond and Bergstrom, 2006). The incandescent cut off diameter of SP2 is 70 nm and SP2 measures BC core size ranges from 70 to 500 nm for a density of 1800 kg/m^3.

AMS unit mass resolution (UMR) data was analyzed in the SQUIRREL software package (version 1.54) and the HR analysis was performed by using PIKA (version 1.13) with the help of peak fitting algorithm (DeCarlo et al., 2006) to derive the mass concentration of organics and inorganics. These analyzing tools were developed in IGOR Pro 6.22A (Wavemetrics) software.

The quantitative accuracy of AMS depends on its collection efficiency (CE). The collection efficiency of AMS can be affected by the bouncing of particle from the vaporizer surface that varies with the chemical composition of aerosol, which contributes to the uncertainty in CE of AMS. Previous studies at the same sampling site (Bhattu and Tripathi, 2015; Chakraborty et al., 2015; Shamjad et al., 2016, 2015) used the chemically dependent CE as mentioned in (Middlebrook et al., 2012), and (Chakraborty et al., 2015) identified that a CE of 0.5 showed a good agreement between mass concentration of SMPS and AMS. Thus a constant CE of 0.5 was selected for the present study (Middlebrook et al., 2012) as it accounts for the acidity, chemical composition of aerosols and RH of the aerosol at the inlet of AMS. Standard air

fragmentation table adjustments were performed at *m/z* values of 16 (O^+), 29 ($N_{15}N^+$) and 44 ($CO_2{}^+$) by using HEPA filter. UMR difference spectra (signal-background) were calculated while HEPA filter was connected to AMS.

These corrected high resolution (HR) mass concentration of organics fitted with peak fitting algorithm (DeCarlo et al., 2006) were further processed using positive matrix factorization (PMF) (Paatero and Tapper, 1994) to determine the mass concentration of various organic species. The mass fraction variation of (mass of the species/total organic mass) each of these species was used further to understand its effect on BC mixing state. Details of PMF analysis are elaborated in the subsequent paragraph. PASS-3 derived absorption coefficient at 781 nm was further averaged to hourly values and converted to mass absorption cross-section (MAC_{781}) by using the hourly averaged mass concentration retrieved from SP2. Along with these instruments, incoming solar flux was measured using a pyranometer which is a part of Aerosol Robotic Network (AERONET) (Kaul et al., 2011; Singh et al., 2004) and located in the vicinity of the sampling site. The available level 1 solar flux data was further averaged to hourly values. All times reported in this study are local time (LT).

PMF was applied to high-resolution (HR) AMS organic mass spectra and one to nine factors were selected to identify the optimum solution (Fig. S2 (a)). A five-factor solution was chosen on the basis of its Q/Q_{exp} values, residuals and its correlation with the external factors (Fig. S2 (b)). The five factors of HR-PMF were cooking organic aerosol (COA), biomass burning organic aerosol (BBOA), low volatile oxygenated organic aerosol (LVOOA) and two mixed factors where BBOA is mixed with primary emissions (POA-BBOA) and oxygenated organic aerosols (OOA-BBOA) shown in Fig. 2.

Previous studies in IGP also observed oxidized BBOA factors (Chakraborty et al., 2015) where the BBOA was aged and oxygenated by atmospheric processing. The OOA- BBOA factor in the present study (O/C = 0.91) was well correlated with *m/z* 44 measured by AMS ($CO_2{}^+$, R^2 = 0.75) and with the tracers of BBOA i.e. *m/z* 60 ($C_2H_4O_2{}^+$, R^2 = 0.80), *m/z* 73 ($C_3H_5O_2{}^+$, R^2 = 0.84). The LVOOA factor (O/C = 1.11) was correlated well with $CO_2{}^+$ (R^2 = 0.55) and $SO_4{}^{2-}$ (R^2 = 0.41). The COA factor (O/C = 0.33, H/C = 1.64) was correlated well with *m/z* 55 ($C_4H_7{}^+$, R^2 = 0.63) and *m/z* 57 ($C_4H_9{}^+$, R^2 = 0.67), but a higher relative intensity at *m/z* 55 indicates the significant COA contribution with respect to HOA. Previous studies also reported the difficulties in separating COA from HOA and observed that these POA occurred as a mixed factor in PMF (Chakraborty et al., 2015; He et al., 2010, 2011a). BBOA factor was correlated well with *m/z* 60 ($C_2H_4O_2{}^+$, R^2 = 0.72) and *m/z* 73 ($C_3H_5O_2{}^+$, R^2 = 0.70).

Previously (Bhattu and Tripathi, 2015) identified oxygenated primary organic aerosol in IGP which showed a higher O/C ratio than primary organic aerosols (POA) due to the mixing of BBOA with POA. A similar POA-BBOA factor was identified in the present study where BBOA was mixed with POA. POA-BBOA factor was correlated well with *m/z* 57 ($C_4H_9{}^+$, R^2 = 0.51) and *m/z* 60 ($C_2H_4O_2{}^+$, R^2 = 0.55). The limitations of elemental analysis of AMS have discussed elsewhere (Aiken et al., 2007).

3. Results and discussion

3.1. Refractory black carbon (BC) mass and number concentrations

Hourly averaged BC mass concentration for the entire winter period showed a large variability from 0.73 μg/m^3 to 17.05 μg/m^3 (Fig. S6), with a mean and standard deviation of 4.06 ± 2.46 μg/m^3. The diurnal variation of BC mass concentration (Fig. 3) showed that the mass concentration increased both in the morning and in late nights as observed in other studies (Begam et al., 2016; Kalluri et al., 2017; Singh et al., 2015). The diurnal trend was 'single peak and valley' pattern and was different from the 'two peaks and two valleys' pattern observed in previous studies (Wang et al., 2016, 2014a). The present study observed a distinct wider and deeper valley in daytime i.e. between 8:00 and 17:00 LT and a prominent peak in nighttime i.e. between 17:00 and 8:00 LT. The BC mass concentration was nearly constant in between (6:00 to 8:00 LT) which was different from the remaining diurnal trend, where the change in BC concentration was clearly visible. This could be due to the balancing of the decrease in BC concentration due to boundary layer expansion by the increase in BC loading from vehicular emissions at early morning period.

The BC mass concentration reached its maximum value between 22:00 and 2:00 LT and nighttime BC concentration characterized by higher standard deviations than the day (8:00 to 17:00 LT). The difference between mean and median was higher at night than day. Specifically, this difference was gradually increasing between 22:00 to 24:00 LT indicating an event driven BC loading. This increase in event driven BC loading can be correlated with the fresh BC emission from biomass burning events near the sampling location. The mean-median difference peaked between 4:00 to 6:00 LT that can be correlated with early morning burning events.

A very good positive correlation between BC mass concentration (r = 0.98) and number concentration (Fig. S1) from SP2 indicate that the number of BC particles per unit BC mass showed very low variability during the entire sampling period. The BC number concentration varied from 277 #/cm^3 to 5865 #/cm^3 during the sampling period. Previous studies at this site showed that the persistent stable weather conditions (i.e. calm winds), shallow boundary layer (Nair et al., 2007), enhanced biomass/trash burning (Ram et al., 2010; Ram and Sarin, 2015) and vehicular emissions (Baxla, 2009) are the potential sources of elevated BC concentration during winter.

To understand the emission characteristics of BC, its mass concentration was correlated with the mass concentration of inorganics and organic aerosol (OA) factors and observed that mass concentration of BC and chloride (Cl^-) were positively correlated (r = 0.47). The previous study indicated that trash burning could emit a significant amount of Cl^- into the atmosphere (Li et al., 2012). Trash burning, particularly in winter, was common phenomena and our findings suggest that it could contribute to total BC emissions in IGP during the winter season. Also, a good positive correlation of BC with COA (r = 0.55), POA-BBOA (r = 0.44), BBOA (r = 0.54) indicated that biomass burning and POA emissions could also emit BC into the atmosphere. A good positive correlation of COA with BC might be due to the presence of HOA fraction in the factor profile of COA.

3.2. Fraction of thickly coated BC

Aging process of BC can change its morphology and structure. Even though the aging of BC can form various morphological configurations (Adachi et al., 2014; Adachi and Buseck, 2008; China et al., 2013; Fu et al., 2012; Moffet et al., 2016; Ueda et al., 2016), the present study assumes an internally mixed structure with BC core and a shell of organics and inorganics (Bond and Bergstrom, 2006). Internal mixing of BC with these species (organics and inorganics) can change its hygroscopicity (Khalizov et al., 2009; Oshima et al., 2009) which has significant implications for radiative forcing (Jacobson, 2001; Liu et al., 2013; Shamjad et al., 2015). The number fraction of "thickly coated BC" particles (fTC_{BC}) over the study period varied from 23.8 to 79.7%, with a mean and standard deviation of 61.6 ± 9.8%. The higher mean fTC_{BC} indicated the prevalence of internally mixed BC fraction at our site during the winter period. The diurnal variation of fTC_{BC} (Fig. 4) showed that the fTC_{BC} increased between 08:00 LT to 18:00 LT. The increased fTC_{BC} after sunrise, with peaking at about 14:00 LT, could be attributed to the formation of the secondary organic aerosol (SOA) with enhanced photochemical activities around noon local time (Chang and Lee, 2007; Jiang et al., 2016). Formation of SOA along with high RH conditions (Li et al., 2017), especially during the foggy period, can further enhance the internal mixing of BC (Kaul et al., 2011; Ram et al., 2012b).

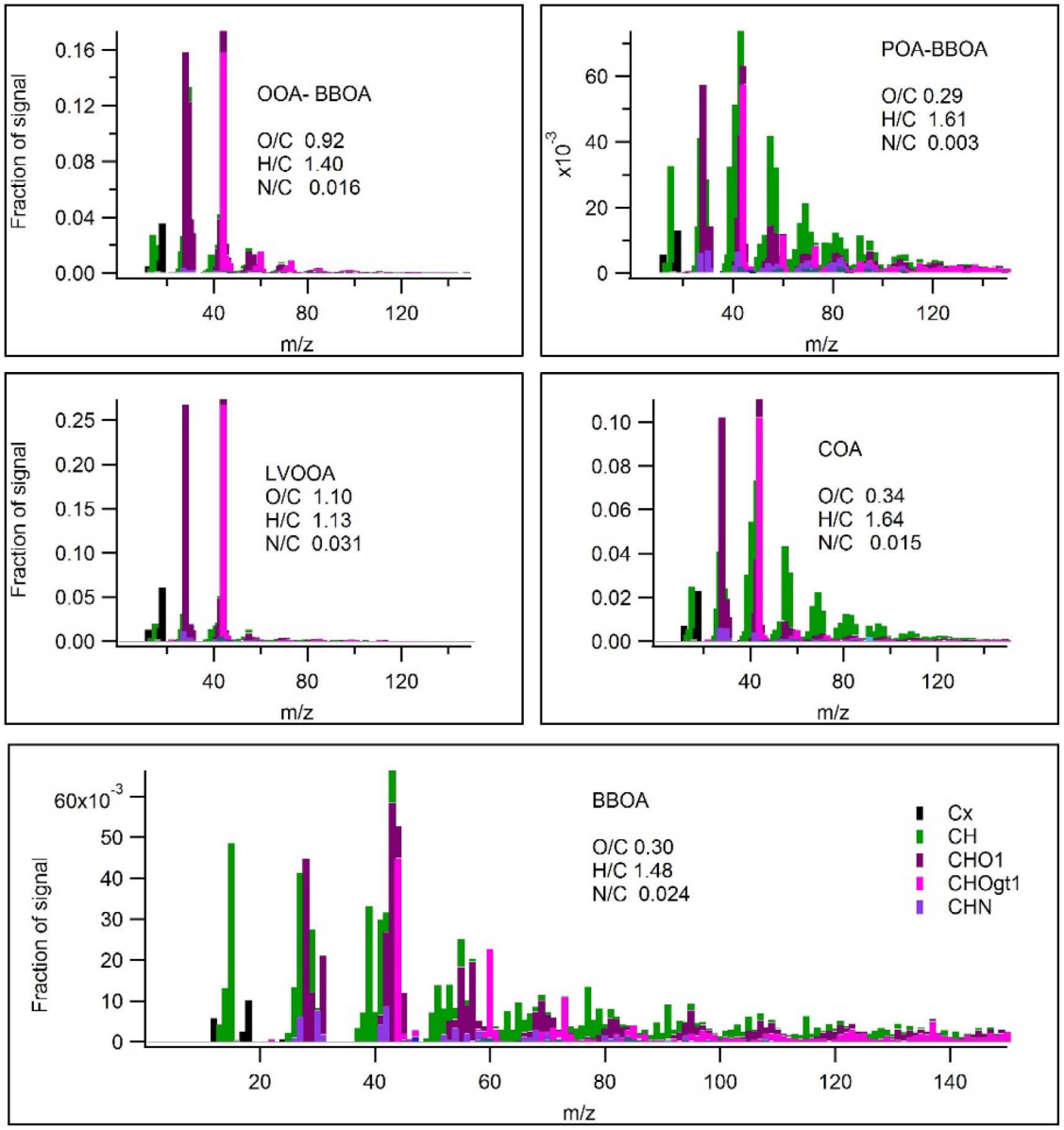

Fig. 2. Factor profiles of HR- PMF analysis. OOA-BBOA = oxidized organic aerosol with significant biomass burning factors, COA = Cooking OA (primary OA), BBOA = biomass burning OA, and POA-BBOA = Primary OA with significant BBOA fraction, LVOOA = low volatile oxygenated OA.

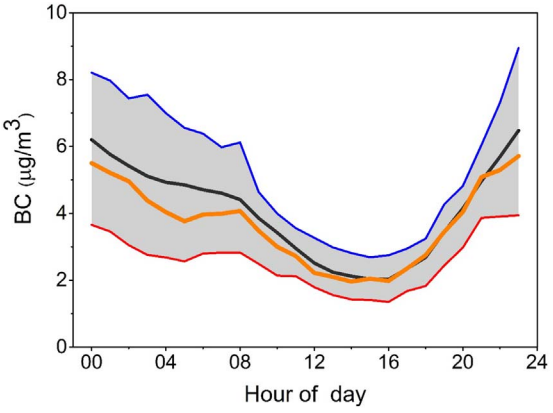

Fig. 3. Diurnal variation of mass concentration of BC. The top blue and bottom red lines indicate 75 and 25 percentiles, respectively. The black and orange lines indicate the mean and median BC concentration. (For interpretation of the references to colour in this figure legend, the reader is referred to the web version of this article.)

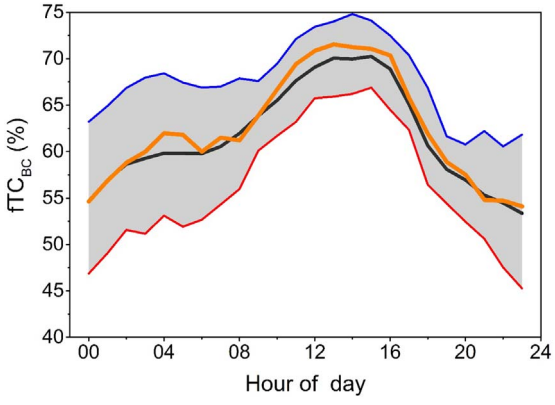

Fig. 4. Diurnal variation of number fraction of "thickly coated BC" particles (fTC_{BC}). The top blue and bottom red lines indicate 75 and 25 percentiles, respectively. The black and orange lines indicate the mean and median fTC_{BC}. (For interpretation of the references to colour in this figure legend, the reader is referred to the web version of this article.)

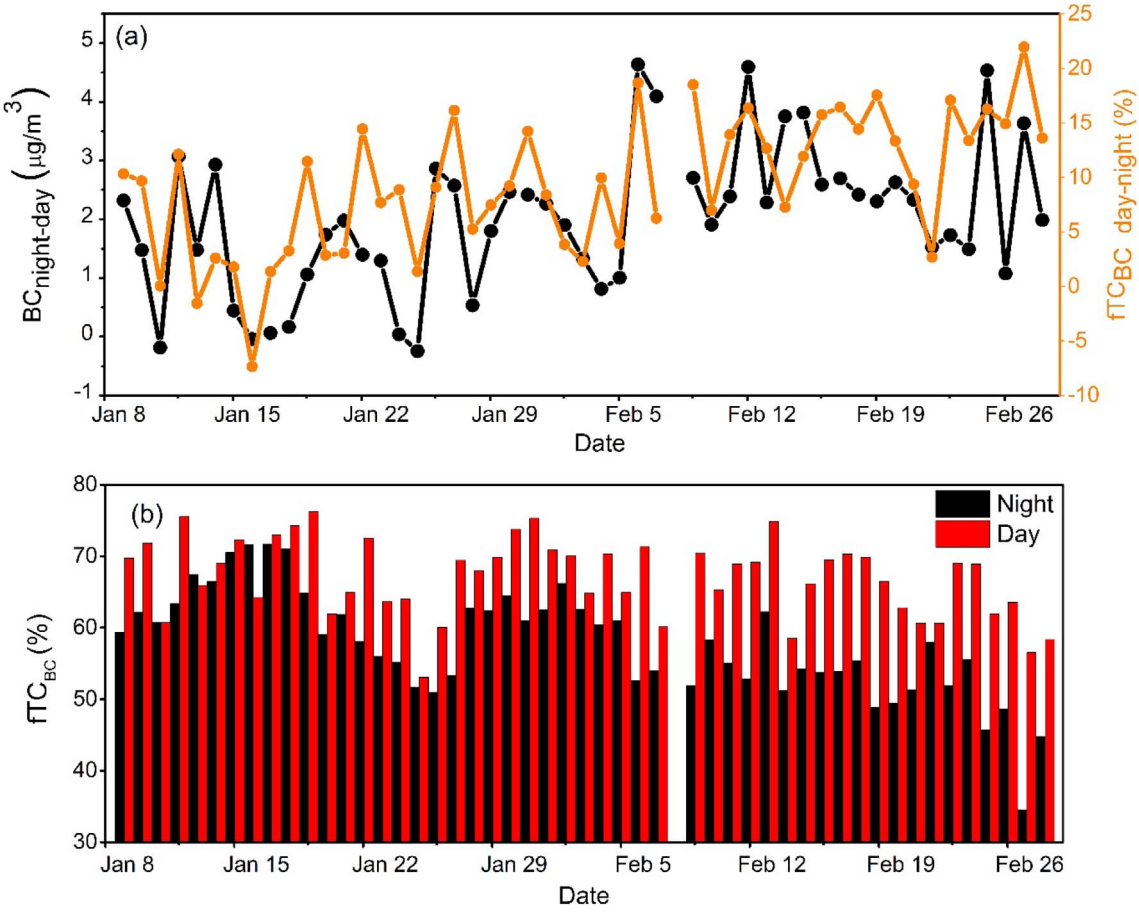

Fig. 5. Variation of (a) $BC_{night\text{-}day}$ and $fTC_{BC\ day\text{-}night}$ and (b) fTC_{BC} day and night (%) during the sampling period.

fTC_{BC} also showed an increase from late night to early morning period (01:00 to 04:00 LT) which can be the result of decreased freshly emitted BC particle during this period (Fig. 3). This increasing trend of fTC_{BC} was discontinued between 04:00 and 06:00 LT, possibly due to the fresh BC emission from early morning biomass/trash burning.

To identify the interaction between BC mixing state and BC mass concentration, the entire winter period data were categorized into the day (08:00 to 17:00 LT) and night (17:00 to 08:00 LT). The difference between night and day BC mass concentration ($BC_{night\text{-}day}$) was plotted along difference in day and night fTC_{BC} ($fTC_{BC\ day\text{-}night}$) (Fig. 5(a)). Biomass burning events at night increase the value of $BC_{night\text{-}day}$ by introducing fresh BC and increasing its mass concentration in IGP. This freshly emitted hydrophobic and externally mixed BC, in turn, reduces the fTC_{BC} in IGP at night and increase $fTCBC_{day\text{-}night}$ value. This positive correlation between $BC_{night\text{-}day}$ and $fTC_{BC\ day\text{-}night}$ can be seen throughout the sampling period (Fig. 5(a)), indicating that fTC_{BC} in IGP was significantly influenced by BC mass concentration.

Also for almost all days, the fTC_{BC} was higher for the day than that the night period (Fig. 5(b)). The mean monthly daytime solar fluxes for January and February were 212.2 W/m^2 and 461.82 W/m^2; this trend had also been reflected in the fTC_{BC} with large differences between day and night values towards the end of the winter season representing the influence of boundary layer dynamics and solar radiation on the fTC_{BC} formation.

Table 1 summarizes calculated fTC_{BC} from different locations and platforms. In IGP, the fTC_{BC} reached as high as 79.7%, and the observed range of fTC_{BC} (23.8–79.7%) was slightly exceeded compared to that of other ground and aircraft-based studies in Asia (Wang et al., 2014a, 2014b) and USA (Metcalf et al., 2012; Schwarz et al., 2008), except that it was much higher than that of the observed range in the UK (McMeeking et al., 2011b).

Table 1
Summary of SP2 estimated fTC_{BC} from various studies.

Location	Site type	Time period (mm/yyyy)	fTC_{BC} (%)	Reference
Kanpur, India	Ground	01/2015–02/2015	23.8–79.7	This study
Xi'an, China	Ground	12/2012–01/2013	18.3–68.8	(Wang et al., 2014a)
Qinghai, China	Ground	10/2011	25–68	(Wang et al., 2014b)
Texas, USA	Aircraft	09/2006	10–70	(Schwarz et al., 2008)
London, UK	Aircraft	04/2008	16–37	(McMeeking et al., 2011b)
Los Angeles, USA	Aircraft	05/2010	29–76	(Metcalf et al., 2012)

3.3. Composition of submicron aerosol internally mixed with BC

Various organic and inorganic aerosols emitted into the atmosphere can significantly affect BC's mixing state and hygroscopicity. These organics are the major fraction of particulate matter < 1 μm (NR-PM_1) by mass and include a large number of species with complex characteristics.

The overall PM_1 composition showed domination of organics (Fig. 6a) in total mass (~61%) followed by NH_4^+, NO_3^- (~11% each), SO_4^{2-} (~10%), BC (~5%) and Cl^- (3%). The PM_1 overall average mass concentration was 87 ± 39 $\mu g/m^3$. The percentage contribution of organic species to total organic mass as derived from the PMF is showed in Fig. 6b. LVOOA contributed approximately 40% to the total organic mass and was the predominant organic species. BBOA, POA-BBBOA, OOA-BBOA, COA were contributed in between 10 and 20%. A higher

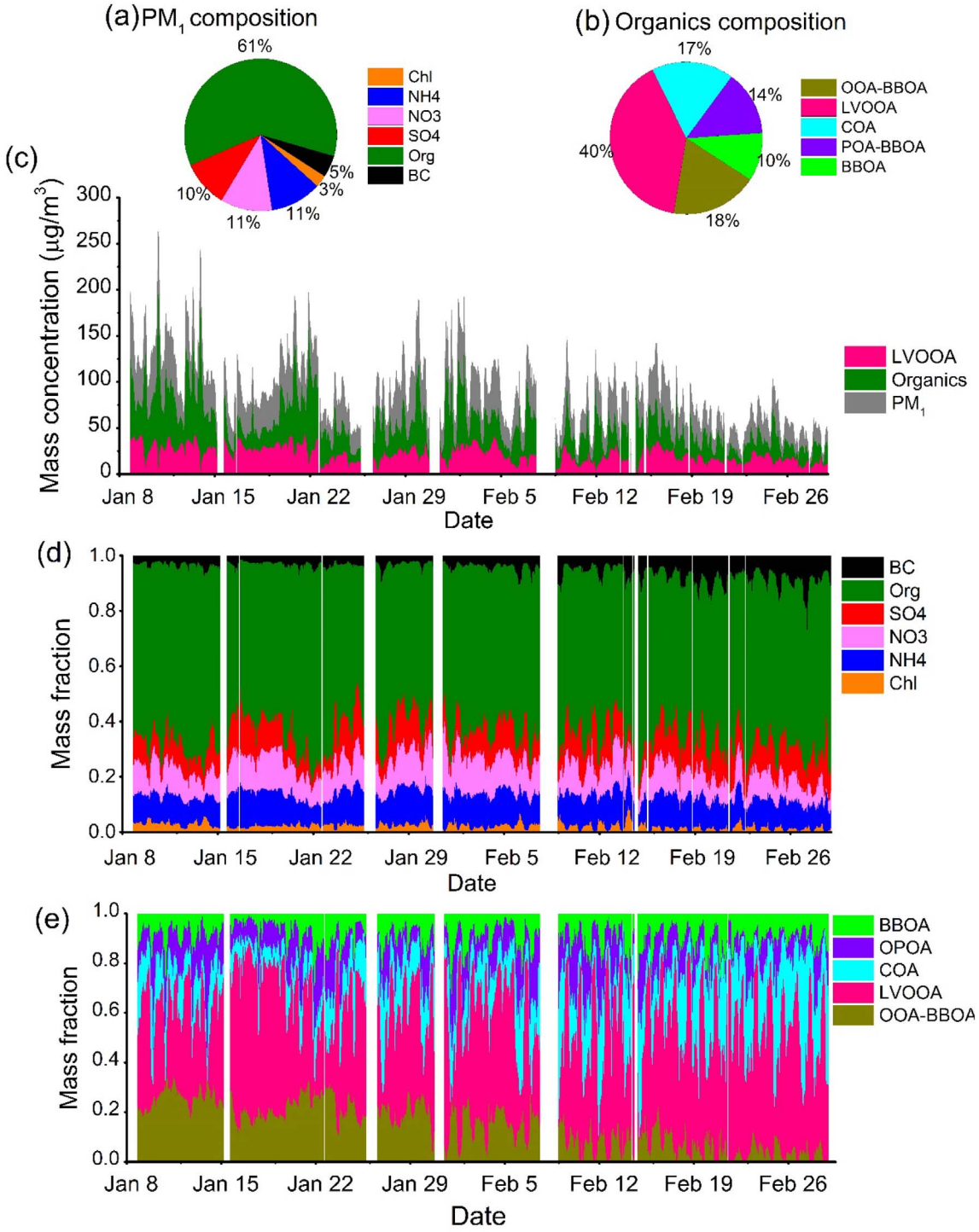

Fig. 6. Time series of non-refractory species and BC (a) and (b) mean composition of PM1 and total organics; (c) indicate the fractional mass concentration of LVOOA, Organics towards the total PM_1 mass concentration; (d) mass fraction of non-refractory species in total PM_1 mass concentration; (e) mass fraction of OA factors towards total organics mass concentration.

fraction of LVOOA in total organic mass indicates that the significant fraction of organic aerosols was aged and oxygenated.

Fig. 6c showed the fractional contribution of LVOOA and organics in the total mass concentration of PM_1. It was evident from the time series that the mass concentrations of PM_1, organics, LVOOA were gradually decreasing from January to February possibly due to the reduction in biomass burning. It was also notable that the mass fraction of BC (Fig. 6d) was gradually increasing towards the end of the sampling period by the compensation of decreased mass fraction of NO_3^- and Cl^-. Previous studies found out that these biomass burning can significantly contribute towards NO_3^- (Lobert et al., 1990) and peroxy nitrates (Aruffo et al., 2016) while garbage burning can contribute towards Cl^- (Li et al., 2012). A reduction in the mass fraction of these inorganic species (Fig. 6d) indicates that the biomass and trash burning was gradually reduced at the end of the sampling period. Mass fraction time series of OOA-BBOA showed decreased OA mass contribution towards the end of the sampling period (Fig. 6e) due to the decreased of long-range transported BBOA emissions.

A diurnal plot of mass concentration of various organic factors obtained from the HR-PMF along with BC mass concentration is shown in

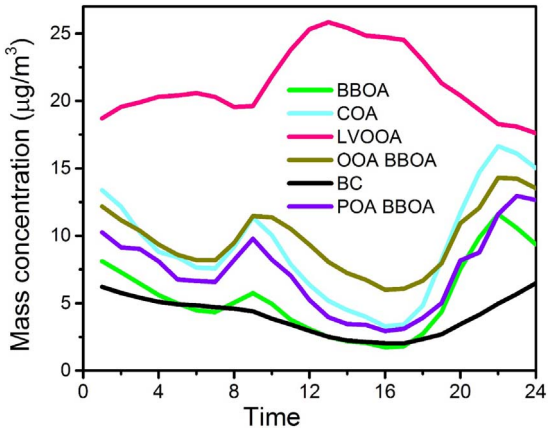

Fig. 7. Diurnal variation of PMF OA factors and BC during the sampling period.

Fig. 7. It was observed that the mass concentration of LVOOA was increasing in the daytime. Previous studies from IGP also reported an increase in oxygenated species in photochemically active periods (Bhattu and Tripathi, 2014; Chakraborty et al., 2015). The similarity between the diurnal trend of LVOOA and fTC_{BC} showed that the coating on BC was influenced by the age of OA and solar photochemistry. Diurnal profiles of other primary organic factors (COA, BBOA, and POA-BBOA) showed a similar trend where their mass concentrations peak at both morning and night and where the contributions from the fresh emission could be significantly higher.

To understand the role of these organic species to form internally mixed BC particles in the atmosphere, the mass fraction (mass of organic factor/mass of total organics) of these species i.e. fBBOA, fCOA, fOOA-BBOA, fPOA-BBOA, fLVOOA were correlated with fTC_{BC}. Primary organic aerosol like COA (Fig. 8a) and BBOA (Fig. 8b) were negatively correlated ($r = -0.78$, $r = -0.51$ respectively) with fTC_{BC} indicating that these OA were locally emitted and primary in nature. These least mixed primary organic aerosols (COA & BBOA) with low O/C ratios (0.34 & 0.30 respectively) also followed the similar diurnal trend with BC, indicating the simultaneous emission of BC, COA, and BBOA in the atmosphere. This simultaneous emission of BC, COA, and BBOA can promote their co-existence as an external mixture with BC and can inversely correlate with the internally mixed BC fraction in IGP. Mixed OA where BBOA was mixed with highly oxygenated species (OOA-BBOA) and with primary organic aerosols (POA-BBOA) (Fig. 8c and d respectively) showed very low correlation ($r = 0.17$, $r = -0.22$, respectively) with fTC_{BC}. The presence of three BBOA factors (BBOA, OOA-BBOA, and POA-BBOA) with different O/C ratios (0.30, 0.90 and 0.29 respectively) indicated the heterogeneity of BBOA in sampling site.

The fLVOOA is an indicator of the mass fraction of highly aged more oxidized OA (Decesari et al., 2014). fLVOOA correlated well ($r = 0.6$) with fTC_{BC} (Fig. 8e) (p-value < 0.001, highly significant) indicating that an increase in this highly oxygenated aerosols (O/C = 1.1) could enhance the internal mixing of BC by its condensation on BC, which is also evident from the diurnal trend of fTCBC and fLVOOA (Figs. 4 & 7). As fLVOOA contribute significantly (up to 86% of total OA mass) during the sampling period (Fig. 6(e)), a hypothetical extrapolation was done to understand the maximum fTC_{BC} that can be reached in an environment where LVOOA contribute the complete OA (fLVOOA = 1). The extrapolation of fLVOOA from 0 to 1 can significantly increase the fTC_{BC} from 47.1 to 78.6% in IGP. Previous papers reported that LVOOA could promote the production and growth of internally mixed BC under the effect of photochemical aging through condensation of this oxygenated organic aerosol (Cappa et al., 2012). It was also evident from the linear regression (Fig. 8e) that an increase in 10% of LVOOA in OA could increase fTC_{BC} by 3.15% at our site.

During atmospheric aging BC undergoes significant compaction and structural modification (He et al., 2015, 2011b; Saathoff et al., 2003; Weingartner et al., 1997; Zhang et al., 2008) which changes its morphology in the atmosphere (Adachi et al., 2014; Adachi and Buseck, 2008; China et al., 2013; Moffet et al., 2016). A two stage of morphological modification of BC where compaction followed by significant non-refractory coating together can enhance the absorption by a factor of 2.4 in a shorter aging time scale of 4.6 h in China (Gustafsson and Ramanathan, 2016; Peng et al., 2016). The increase in the fTC_{BC} during the daytime further suggested that most of the coating on BC could be largely attributed to LVOOA and possibly could be the main contributor of 'short time' aging of BC and enhancement of absorption.

To understand the effect of inorganic concentration on BC mixing state, the mass fraction of nitrate, sulfate, chloride, and ammonium was correlated with fTC_{BC}. Among inorganics, nitrate and ammonium were correlated positively with fTC_{BC} ($r = 0.47$, $r = 0.58$ respectively) indicating that these inorganic species can also form a coating over BC (Fig. 9).

Mass size distribution of BC was compared with organic proxies to understand their relative distributions and mode (Fig. 10). SP2 provides the mass distribution of volume equivalent diameter of BC (d_{ve}) correspondent to a void-free particle density (ρ_p) of 1800 kg/m^3. This d_{ve} of BC needs to convert into vacuum aerodynamic diameter (d_{va}) to compare with the organics proxies for which shape factor of BC (χ) is an important parameter as BC shows significantly varying morphologies in the atmosphere (Adachi et al., 2014; Adachi and Buseck, 2008; China et al., 2013; Moffet et al., 2016).

However, the details of morphological features of BC were not available during the sampling period. To address this limitation, the study assumed a concentric core-shell structure with a χ equals to 1 for ambient BC (Bond and Bergstrom, 2006) as the majority of BC in the sampling site was internally mixed ($\approx 62\%$). Assuming $\chi = 1$ and standard density of particle $\rho_0 = 1000$ kg/m^3, the volume equivalent diameter (d_{ve}) of BC estimated from SP2 was converted to vacuum aerodynamic diameter (d_{va}) by the Eq. (1) (DeCarlo et al., 2004).

$$d_{Va} = \frac{\rho_p d_{ve}}{\rho_0 \chi} \quad (1)$$

The mass size distribution of *m/z* 43 (a proxy for SVOOA), *m/z* 44 (a proxy for LVOOA), *m/z* 55, *m/z* 57 (proxies for POA), *m/z* 60 and *m/z* 73 (proxies for BBOA) were plotted along with the mass size distribution of BC from SP2. The mode of the size distribution of these organic proxies was in the accumulation mode, ranging from 384 nm (*m/z* 57) to 620 nm (*m/z* 44). The higher atmospheric aging and oxidation of LVOOA might be contributing its higher size distribution mode than other organic proxies.

To understand the distribution of BC mass and number compared to total PM_1 species, mass and number size distribution of BC cores were plotted along with scanning mobility particle sizer (SMPS) derived mass and number distribution of PM_1 (Fig. S5). While the modal diameter of BC and PM_1 number size distribution showed similar modes (approximately at 100 nm), mass size distribution mode for BC and SMPS showed different modes i.e.180 nm and 400 nm respectively. The mass size distributions were performed at a density of 1800 kg/m^3 for BC and 1200 kg/m^3 for PM_1 aerosols.

3.4. BC mixing state and light absorption properties

The mass absorption cross-section (MAC) of BC is an important parameter to understand the radiative forcing calculations (Khalizov et al., 2009; Wang et al., 2014a). The aging of BC can increase the non-refractory coating on its surface and this coating can increase the MAC (Subramanian et al., 2010) which can further make BC more absorbing due to morphological change (Liu et al., 2015) and lensing effect (Cappa et al., 2012).

Absorption coefficient (βabs) at a wavelength of 781 nm of PASS-3 was selected to calculate the mass absorption cross-section of BC

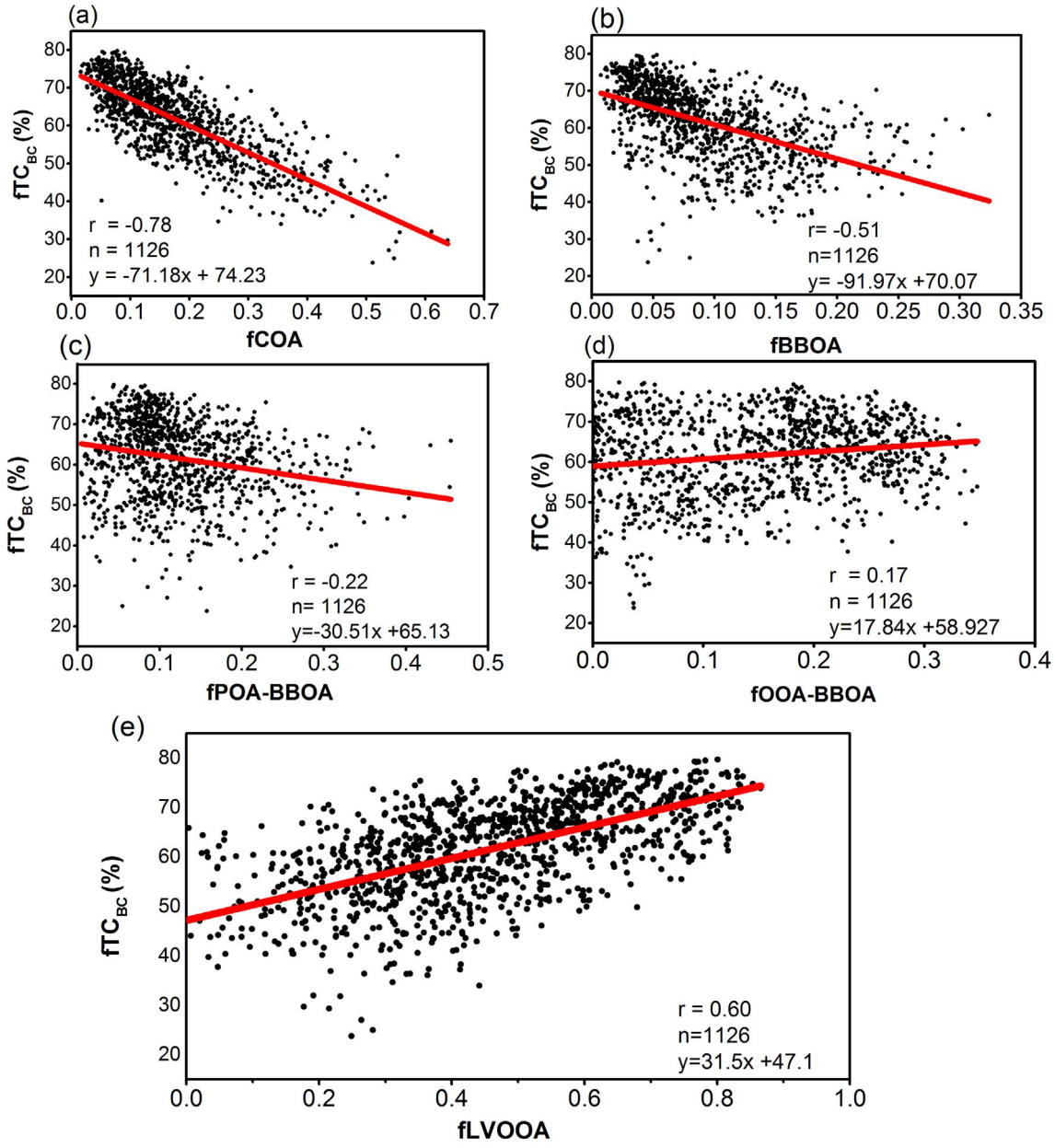

Fig. 8. Scatter plot of fraction of primary OA factors ((a) fCOA, (b) fBBOA) and mixed factors ((c) fPOA-BBOA, (d) fOOA-BBOA), (e) fLVOOA with fTC_{BC}.

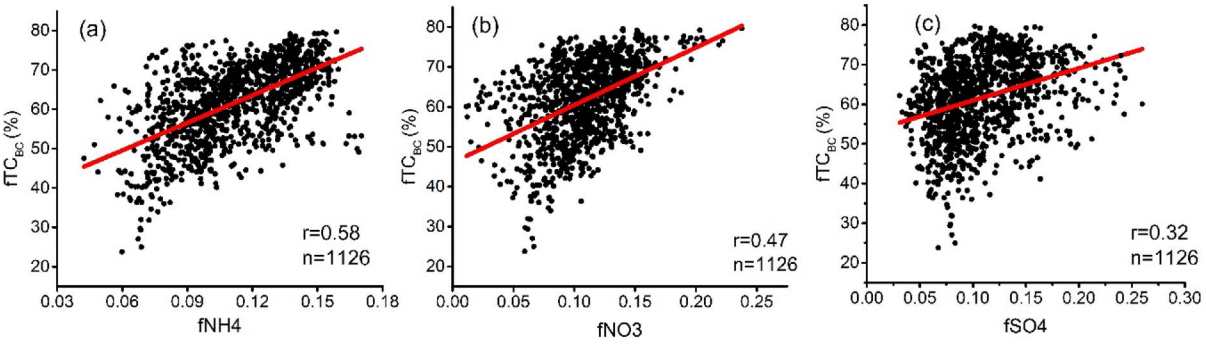

Fig. 9. Scatter plot of the mass fraction of ammonium (a), nitrate (b) and sulfate (c) with $fTC_{BC.}$ fNH_4, fNO_3, fSO_4 indicate the mass fraction of ammonium, nitrate, and sulfate respectively.

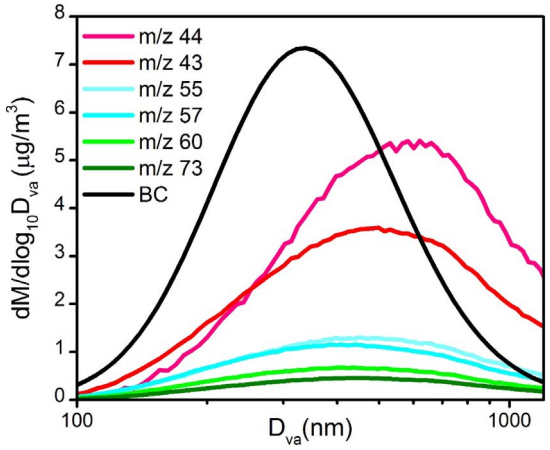

Fig. 10. Mass size distribution of organic proxies and BC.

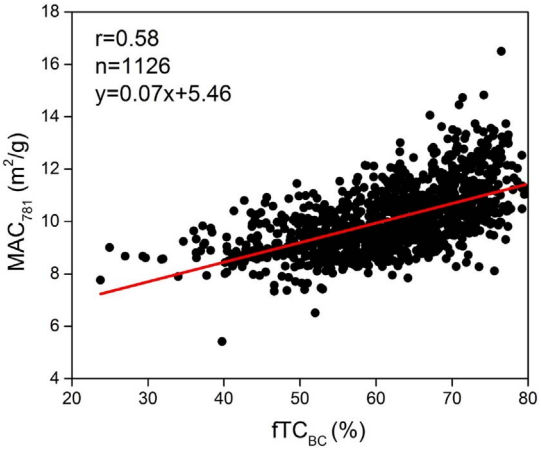

Fig. 11. Scatter plot between fTC_{BC} and the MAC_{781}.

particles, hereafter referred to as MAC_{781}. Previous studies also correlated the interaction between MAC values with fTC_{BC} (McMeeking et al., 2011b; Wang et al., 2014a). The MAC_{781} (m^2/g) was calculated by using the relationship connecting β_{abs} and BC mass concentration [BC] (Eq. (2)) which was used by (Wang et al., 2014a).

$$\beta abs(total) = MAC \times [BC] + \beta_{others} \quad (2)$$

where β_{others} is the absorption from non-BC particles.

As absorption contribution from the brown carbon species is negligible at 781 nm (Shamjad et al., 2016, 2015) and BC is the main absorbing aerosol at a higher wavelength (Ramachandran and Rajesh, 2007; Wang et al., 2014a), β_{others} is assumed to zero. A very good correlation between [BC] and β_{abs} was observed (r = 0.97) which was plotted in Fig. S4 (a). The Gaussian curve fitted to the frequency distribution of MAC for the entire sampling period was shown in Fig. S4 (b). The mean ± standard deviation of the β_{abs} and MAC for the sampling period were 39.5 ± 22 Mm^{-1} and 10.1 ± 1.27 m^2/g respectively. (Bond and Bergstrom, 2006) compared many studies involving MAC calculation and identified that the MAC values can vary up to a factor of four, i.e. 5–20 m^2/g and proposed a MAC of 7.5 ± 1.2 m^2/g at 550 nm for uncoated particles.

Table 2. Indicate the SP2 based MAC calculation around the globe. The studies were performed both on the ground and in aircraft. The MAC values showed wider range from 7.6m^2/g to 15.4 m^2/g in the studies. The inverse relation of MAC with wavelength (Bond and Bergstrom, 2006; Ram et al., 2012b) was reflected in the observed MAC values around the globe. The observed MAC values at Mexico and Switzerland were much comparable to the MAC values of our sampling site as the MAC measurement was made at the nearby wavelength.

Enhancement of absorption due to the secondary organic aerosol coating on BC is still debatable points. (Cappa et al., 2012; Lan et al., 2013; Nakayama et al., 2014) in their recent studies identified that the climate models were overestimating the absorption and observed a lesser enhancement of approximately 6–10% in their studies. (Shamjad et al., 2016; Ueda et al., 2016) observed a moderate enhancement in absorption by a factor of 1.2–1.3 and (Ueda et al., 2016) observed an enhancement > 1.3 for long-range transported air mass. On the contrary, (Liu et al., 2015; Wang et al., 2014a) observed a significant enhancement in absorption by a factor of 1.5–1.8 in their studies.

To recognize the variation of mass absorption with mixing the state of BC in our sampling site, a scatter plot of fTC_{BC} and MAC was plotted (Fig. 11). fTC_{BC} was positively correlated (r = 0.58, p < 0.005) with the MAC, suggesting that the increase in the fTC_{BC} makes BC more absorbing at a wavelength of 781 nm. The extrapolation of the linear regression to purely externally mixed conditions (fTC_{BC} = 0%) corresponded to an MAC_{781} of 5.46 m^2/g and MAC_{781} increased to 12.46 m^2/g when BC was completely internally mixed (fTC_{BC} = 100%). This indicates that the MAC_{781} was enhanced by a factor of 2.28 when a pure externally mixed BC was converted to a completely internally mixed BC. The uncertainty in fTC_{BC} for the entire campaign period was 16% and the linear extrapolation of the correlation between fTC_{BC} and MAC_{781} contributes to an uncertainty in slope (4%) and intercept (3%) (Fig. 11). These uncertainties in fTC_{BC}, slope, and intercept can together contribute to an uncertainty of 8% in the MAC_{781} calculation in the sampling period. The observed average value of fTC_{BC} was 61.6%, which would enhance the MAC by a factor of 1.8 at our site.

4. Conclusions

This study presents the mass, number concentration and mixing state of BC at an urban location, Kanpur, in IGP during the winter of 2015–16. We also investigated how organic and inorganic non-refractory species can influence BC mixing state and the impact on the mass absorption cross-section. SP2 and PASS-3 were used to identify the mixing state and absorption property of BC respectively, while AMS was used to identify the non-refractory mass concentrations.

Mass, number concentration of BC showed a distinct peak at night due to the increased anthropogenic emissions from biomass/trash burning and prevailing stable weather conditions. The mean BC mass and number concentration for the entire study period was 4.06 $\mu g/m^3$,

Table 2
Summary of SP2 BC mass concentration derived MAC_λ from various studies. PAX refers to Photoacoustic Extinctiometer. MAAP and PSAP refer to Multi-Angle Absorption Photometer and Particulate Soot Absorption Photometer. λ (nm) indicates the operating wavelength in nm for the various instruments.

Location	Site type	Time period (mm/yyyy)	β_{abs} measurement	MAC (m^2/g)	λ (nm)	References
Kanpur, India	Ground	01/2015–02/2015	PASS-3	10.08	781	This study
Xi'an, China	Ground	12/2012–01/2013	PAX	7.6	870	(Wang et al., 2014a)
Switzerland	Ground	02–03/2007	MAAP	10.2	630	(Liu et al., 2010)
Qinghai, China	Ground	11/2012	PAX	13.2	532	(Wang et al., 2015)
Mexico, USA	Aircraft	03/2006	PSAP	10.9	660	(Subramanian et al., 2010)
United Kingdom	Aircraft	04/2008	PSAP	15.4	550	(McMeeking et al., 2011b)

1314 #/cm^3 respectively. The mean fTC_{BC} was 61.6%, which indicated a predominant fraction of BC particles was internally mixed. The increase in fTC_{BC} during the daytime indicated that the SOA formation due to solar photochemistry could further promote the internal mixing of BC. Comparison between day and night fTC_{BC} further suggested that solar flux and therefore photochemistry plays an important role in BC mixing.

Mass fractions of various organic aerosol species were correlated with fTC_{BC} to understand their effect on the mixing state of BC. PMF resolved POA (COA, BBOA) were negatively correlated with fTC_{BC} while LVOOA showed a positive correlation (r = 0.6) with fTC_{BC}, indicating that the BC was coated with highly aged LVOOA fractions. Inorganic species mass fractions include nitrate and ammonium (r = 0.47, r = 0.58 respectively) also contribute to the internally mixed BC in the sampling site. The mean MAC_{781} for the sampling period was found to be 10.1 m^2/g and fTC_{BC} was found to be positively corrected with MAC_{781} (r = 0.58). This suggested that the present fTC_{BC} could amplify the MAC_{781} as much as by a factor of 1.8 in IGP during the winter period. This enhancement factor of 1.8 due to internally mixed BC can be used to perform radiative forcing calculations in winter period of Kanpur.

Acknowledgements

We acknowledge the support of Earth System Science Organization, Ministry of Earth Sciences (MoES), Government of India to conduct this research under Monsoon Mission. We acknowledge the support of IIT Kanpur for providing us with HR-ToF-AMS for PG research and teaching. We also acknowledge the support of Ministry of Human Resource Development (No. 3-21/2014-TS.1), Government of India for their support for conducting this research. The in situ observation data used in this study is available from the authors upon request to the corresponding author (snt@iitk.ac.in).

Appendix A. Supplementary data

Supplementary data to this article can be found online at http://dx.doi.org/10.1016/j.atmosres.2017.07.007.

References

Adachi, K., Buseck, P.R., 2008. Internally mixed soot, sulfates, and organic matter in aerosol particles from Mexico City. Atmos. Chem. Phys. 8, 6469–6481. http://dx.doi.org/10.5194/acp-8-6469-2008.

Adachi, K., Zaizen, Y., Kajino, M., Igarashi, Y., 2014. Mixing state of regionally transported soot particles and the coating effect on their size and shape at a mountain site in Japan. J. Geophys. Res. Atmos. 119, 5386–5396. http://dx.doi.org/10.1002/2013JD020880.

Aiken, A.C., DeCarlo, P.F., Jimenez, J.L., 2007. Elemental analysis of organic species with electron ionization high-resolution mass spectrometry. Anal. Chem. 79, 8350–8358. http://dx.doi.org/10.1021/ac071150w.

Andreae, M.O., Gelencsér, A., 2006. Black carbon or brown carbon? The nature of light-absorbing carbonaceous aerosols. Atmos. Chem. Phys. 6, 3131–3148. http://dx.doi.org/10.5194/acp-6-3131-2006.

Arnott, W.P., 2003. Photoacoustic and filter-based ambient aerosol light absorption measurements: instrument comparisons and the role of relative humidity. J. Geophys. Res. 108, 4034. http://dx.doi.org/10.1029/2002JD002165.

Arnott, W.P., Moosmüller, H., Rogers, C.F., Jin, T., Bruch, R., 1999. Photoacoustic spectrometer for measuring light absorption by aerosol: instrument description. Atmos. Environ. 33, 2845–2852. http://dx.doi.org/10.1016/S1352-2310(98)00361-6.

Arnott, W.P., Moosmüller, H., Walker, J.W., 2000. Nitrogen dioxide and kerosene-flame soot calibration of photoacoustic instruments for measurement of light absorption by aerosols. Rev. Sci. Instrum. 71, 4545. http://dx.doi.org/10.1063/1.1322585.

Arnott, W.P., Hamasha, K., Moosmüller, H., Sheridan, P.J., Ogren, J.a., 2005. Towards aerosol light-absorption measurements with a 7-wavelength aethalometer: evaluation with a photoacoustic instrument and 3-wavelength nephelometer. Aerosol Sci. Technol. 39, 17–29. http://dx.doi.org/10.1080/027868290901972.

Aruffo, E., Biancofiore, F., Di Carlo, P., Busilacchio, M., Verdecchia, M., Tomassetti, B., Dari-Salisburgo, C., Giammaria, F., Bauguitte, S., Lee, J., Moller, S., Hopkins, J., Punjabi, S., Andrews, S.J., Lewis, A.C., Palmer, P.I., Hyer, E., Le Breton, M., Percival, C., 2016. Impact of biomass burning emission on total peroxy nitrates: fire plume identification during the BORTAS campaign. Atmos. Meas. Tech. 9, 5591–5606. http://dx.doi.org/10.5194/amt-9-5591-2016.

Baxla, S.P., 2009. Analysis of diurnal and seasonal variation of submicron outdoor aerosol mass and size distribution in a northern Indian city and its correlation to black carbon. Aerosol Air Qual. Res. 9, 458–469. http://dx.doi.org/10.4209/aaqr.2009.03.0017.

Begam, G.R., Vachaspati, C.V., Ahammed, Y.N., Kumar, K.R., Babu, S.S., Reddy, R.R., 2016. Measurement and analysis of black carbon aerosols over a tropical semi-arid station in Kadapa, India. Atmos. Res. 171, 77–91. http://dx.doi.org/10.1016/j.atmosres.2015.12.014.

Bhattu, D., Tripathi, S.N., 2014. Inter-seasonal variability in size-resolved CCN properties at Kanpur, India. Atmos. Environ. 85, 161–168. http://dx.doi.org/10.1016/j.atmosenv.2013.12.016.

Bhattu, D., Tripathi, S.N., 2015. CCN closure study: effects of aerosol chemical composition and mixing state. J. Geophys. Res. Atmos. 120, 766–783. http://dx.doi.org/10.1002/2014JD021978.

Bond, T.C., Bergstrom, R.W., 2006. Light absorption by carbonaceous particles: an investigative review. Aerosol Sci. Technol. 40, 27–67. http://dx.doi.org/10.1080/02786820500421521.

Bond, T.C., Doherty, S.J., Fahey, D.W., Forster, P.M., Berntsen, T., DeAngelo, B.J., Flanner, M.G., Ghan, S., Kärcher, B., Koch, D., Kinne, S., Kondo, Y., Quinn, P.K., Sarofim, M.C., Schultz, M.G., Schulz, M., Venkataraman, C., Zhang, H., Zhang, S., Bellouin, N., Guttikunda, S.K., Hopke, P.K., Jacobson, M.Z., Kaiser, J.W., Klimont, Z., Lohmann, U., Schwarz, J.P., Shindell, D., Storelvmo, T., Warren, S.G., Zender, C.S., 2013. Bounding the role of black carbon in the climate system: a scientific assessment. J. Geophys. Res. Atmos. 118, 5380–5552. http://dx.doi.org/10.1002/jgrd.50171.

Cape, J.N., Coyle, M., Dumitrean, P., 2012. The atmospheric lifetime of black carbon. Atmos. Environ. 59, 256–263. http://dx.doi.org/10.1016/j.atmosenv.2012.05.030.

Cappa, C.D., Onasch, T.B., Massoli, P., Worsnop, D.R., Bates, T.S., Cross, E.S., Davidovits, P., Hakala, J., Hayden, K.L., Jobson, B.T., Kolesar, K.R., Lack, D.A., Lerner, B.M., Li, S.-M., Mellon, D., Nuaaman, I., Olfert, J.S., Petäjä, T., Quinn, P.K., Song, C., Subramanian, R., Williams, E.J., Zaveri, R.A., 2012. Radiative absorption enhancements due to the mixing state of atmospheric black carbon. Science 337, 1078–1081. http://dx.doi.org/10.1126/science.1223447.

Chakraborty, A., Bhattu, D., Gupta, T., Tripathi, S.N., Canagaratna, M.R., 2015. Real-time measurements of ambient aerosols in a polluted Indian city: sources, characteristics, and processing of organic aerosols during foggy and nonfoggy periods. J. Geophys. Res. Atmos. 120, 9006–9019. http://dx.doi.org/10.1002/2015JD023419.

Chang, S.C., Lee, C. Te, 2007. Secondary aerosol formation through photochemical reactions estimated by using air quality monitoring data in Taipei City from 1994 to 2003. Atmos. Environ. 41, 4002–4017. http://dx.doi.org/10.1016/j.atmosenv.2007.01.040.

Chen, P., Kang, S., Bai, J., Sillanpää, M., Li, C., 2015. Yak dung combustion aerosols in the Tibetan Plateau: chemical characteristics and influence on the local atmospheric environment. Atmos. Res. 156, 58–66. http://dx.doi.org/10.1016/j.atmosres.2015.01.001.

China, S., Mazzoleni, C., Gorkowski, K., Aiken, A.C., Dubey, M.K., 2013. Morphology and mixing state of individual freshly emitted wildfire carbonaceous particles. Nat. Commun. 4, 2122. http://dx.doi.org/10.1038/ncomms3122.

DeCarlo, P.F., Slowik, J.G., Worsnop, D.R., Davidovits, P., Jimenez, J.L., 2004. Particle morphology and density characterization by combined mobility and aerodynamic diameter measurements. Part 1: theory. Aerosol Sci. Technol. 38, 1185–1205. http://dx.doi.org/10.1080/027868290903907.

DeCarlo, P.F., Kimmel, J.R., Trimborn, A., Northway, M.J., Jayne, J.T., Aiken, A.C., Gonin, M., Fuhrer, K., Horvath, T., Docherty, K.S., Worsnop, D.R., Jimenez, J.L., 2006. Field-deployable, high-resolution, time-of-flight aerosol mass spectrometer. Anal. Chem. 78, 8281–8289. http://dx.doi.org/10.1021/ac061249n.

Decesari, S., Allan, J., Plass-Duelmer, C., Williams, B.J., Paglione, M., Facchini, M.C., O'Dowd, C., Harrison, R.M., Gietl, J.K., Coe, H., Giulianelli, L., Gobbi, G.P., Lanconelli, C., Carbone, C., Worsnop, D., Lambe, A.T., Ahern, A.T., Moretti, F., Tagliavini, E., Elste, T., Gilge, S., Zhang, Y., Dall'Osto, M., 2014. Measurements of the aerosol chemical composition and mixing state in the Po Valley using multiple spectroscopic techniques. Atmos. Chem. Phys. 14, 12109–12132. http://dx.doi.org/10.5194/acp-14-12109-2014.

Dey, S., Tripathi, S.N., Singh, R.P., Holben, B.N., 2005. Seasonal variability of the aerosol parameters over Kanpur, an urban site in Indo-Gangetic basin. Adv. Space Res. 36, 778–782. http://dx.doi.org/10.1016/j.asr.2005.06.040.

Dey, S., Tripathi, S.N., Mishra, S.K., 2008. Probable mixing state of aerosols in the Indo-Gangetic Basin, northern India. Geophys. Res. Lett. 35, L03808. http://dx.doi.org/10.1029/2007GL032622.

Draxler, R., Stunder, B., Rolph, G., Stein, A., Taylor, A., 2016. HYSPLIT4 User's Guide HYSPLIT4 USER's GUIDE Version 4 – (Last Revision: February 2016 1).

Fu, H., Zhang, M., Li, W., Chen, J., Wang, L., Quan, X., Wang, W., 2012. Morphology, composition and mixing state of individual carbonaceous aerosol in urban Shanghai. Atmos. Chem. Phys. 12, 693–707. http://dx.doi.org/10.5194/acp-12-693-2012.

Gao, R.S., Schwarz, J.P., Kelly, K.K., Fahey, D.W., Watts, L.a., Thompson, T.L., Spackman, J.R., Slowik, J.G., Cross, E.S., Han, J.-H., Davidovits, P., Onasch, T.B., Worsnop, D.R., 2007. A novel method for estimating light-scattering properties of soot aerosols using a modified single-particle soot photometer. Aerosol Sci. Technol. 41, 125–135. http://dx.doi.org/10.1080/02786820601118398.

Gong, X., Zhang, C., Chen, H., Nizkorodov, S.A., Chen, J., Yang, X., 2016. Size distribution and mixing state of black carbon particles during a heavy air pollution episode in Shanghai. Atmos. Chem. Phys. 16, 5399–5411. http://dx.doi.org/10.5194/acp-16-5399-2016.

Gustafsson, Ö., Ramanathan, V., 2016. Convergence on climate warming by black carbon aerosols. Proc. Natl. Acad. Sci. 113, 201603570. http://dx.doi.org/10.1073/pnas.

1603570113.
He, L.-Y., Lin, Y., Huang, X.-F., Guo, S., Xue, L., Su, Q., Hu, M., Luan, S.-J., Zhang, Y.-H., 2010. Characterization of high-resolution aerosol mass spectra of primary organic aerosol emissions from Chinese cooking and biomass burning. Atmos. Chem. Phys. 10, 11535–11543. http://dx.doi.org/10.5194/acp-10-11535-2010.
He, L.Y., Huang, X.F., Xue, L., Hu, M., Lin, Y., Zheng, J., Zhang, R., Zhang, Y.H., 2011a. Submicron aerosol analysis and organic source apportionment in an urban atmosphere in Pearl River Delta of China using high-resolution aerosol mass spectrometry. J. Geophys. Res. Atmos. 116, 1–15. http://dx.doi.org/10.1029/2010JD014566.
He, L.Y., Huang, X.F., Xue, L., Hu, M., Lin, Y., Zheng, J., Zhang, R., Zhang, Y.H., 2011b. Submicron aerosol analysis and organic source apportionment in an urban atmosphere in Pearl River Delta of China using high-resolution aerosol mass spectrometry. J. Geophys. Res. Atmos. 116, D12304. http://dx.doi.org/10.1029/2010JD014566.
He, C., Liou, K.N., Takano, Y., Zhang, R., Levy Zamora, M., Yang, P., Li, Q., Leung, L.R., 2015. Variation of the radiative properties during black carbon aging: theoretical and experimental intercomparison. Atmos. Chem. Phys. 15, 11967–11980. http://dx.doi.org/10.5194/acp-15-11967-2015.
Jacobson, M.Z., 2001. Strong radiative heating due to the mixing state of black carbon in atmospheric aerosols. Nature 409, 695–697. http://dx.doi.org/10.1038/35055518.
Jayne, J.T., Leard, D.C., Zhang, X., Davidovits, P., Smith, K.a., Kolb, C.E., Worsnop, D.R., 2000. Development of an aerosol mass spectrometer for size and composition analysis of submicron particles. Aerosol Sci. Technol. 33, 49–70. http://dx.doi.org/10.1080/027868200410840.
Jiang, R., Tan, H., Tang, L., Cai, M., Yin, Y., Li, F., Liu, L., Xu, H., Chan, P.W., Deng, X., Wu, D., 2016. Comparison of aerosol hygroscopicity and mixing state between winter and summer seasons in Pearl River Delta region, China. Atmos. Res. 169, 160–170. http://dx.doi.org/10.1016/j.atmosres.2015.09.031.
Jimenez, J.L., Jayne, J.T., Shi, Q., Kolb, C.E., Worsnop, D.R., Yourshaw, I., Seinfeld, J.H., Flagan, R.C., Zhang, X., Smith, K.A., Morris, J.W., Davidovits, P., 2003. Ambient aerosol sampling using the Aerodyne Aerosol Mass Spectrometer. J. Geophys. Res. 108, 8425. http://dx.doi.org/10.1029/2001jd001213.
Kalluri, R.O.R., Gugamsetty, B., Kotalo, R.G., Nagireddy, S.K.R., Tandule, C.R., Thotli, L.R., Shaik, N.H., Maraka, V.R., Rajuru, R.R., Surendran Nair, S.B., 2017. Seasonal variation of near surface black carbon and satellite derived vertical distribution of aerosols over a semi-arid station in India. Atmos. Res. 184, 77–87. http://dx.doi.org/10.1016/j.atmosres.2016.09.003.
Kanawade, V.P., Tripathi, S.N., Bhattu, D., Shamjad, P.M., 2014. Sub-micron particle number size distributions characteristics at an urban location, Kanpur, in the Indo-Gangetic Plain. Atmos. Res. 147–148, 121–132. http://dx.doi.org/10.1016/j.atmosres.2014.05.010.
Kaul, D.S., Gupta, T., Tripathi, S.N., Tare, V., Collett, J.L., 2011. Secondary organic aerosol: a comparison between foggy and nonfoggy days. Environ. Sci. Technol. 45, 7307–7313. http://dx.doi.org/10.1021/es201081d.
Khalizov, A.F., Xue, H., Wang, L., Zheng, J., Zhang, R., 2009. Enhanced light absorption and scattering by carbon soot aerosol internally mixed with sulfuric acid. J. Phys. Chem. A 113, 1066–1074. http://dx.doi.org/10.1021/jp807531n.
Laborde, M., Schnaiter, M., Linke, C., Saathoff, H., Naumann, K.-H., Möhler, O., Berlenz, S., Wagner, U., Taylor, J.W., Liu, D., Flynn, M., Allan, J.D., Coe, H., Heimerl, K., Dahlkötter, F., Weinzierl, B., Wollny, A.G., Zanatta, M., Cozic, J., Laj, P., Hitzenberger, R., Schwarz, J.P., Gysel, M., 2012. Single Particle Soot Photometer intercomparison at the AIDA chamber. Atmos. Meas. Tech. 5, 3077–3097. http://dx.doi.org/10.5194/amt-5-3077-2012.
Laborde, M., Crippa, M., Tritscher, T., Jurányi, Z., Decarlo, P.F., Temime-Roussel, B., Marchand, N., Eckhardt, S., Stohl, A., Baltensperger, U., Prévôt, A.S.H., Weingartner, E., Gysel, M., 2013. Black carbon physical properties and mixing state in the European megacity Paris. Atmos. Chem. Phys. 13, 5831–5856. http://dx.doi.org/10.5194/acp-13-5831-2013.
Lan, Z.J., Huang, X.F., Yu, K.Y., Sun, T. Le, Zeng, L.W., Hu, M., 2013. Light absorption of black carbon aerosol and its enhancement by mixing state in an urban atmosphere in South China. Atmos. Environ. 69, 118–123. http://dx.doi.org/10.1016/j.atmosenv.2012.12.009.
Li, G., Lei, W., Bei, N., Molina, L.T., 2012. Contribution of garbage burning to chloride and PM 2.5 in Mexico City. Atmos. Chem. Phys. 12, 8751–8761. http://dx.doi.org/10.5194/acp-12-8751-2012.
Li, W., Shao, L., Zhang, D., Ro, C.-U., Hu, M., Bi, X., Geng, H., Matsuki, A., Niu, H., Chen, J., 2016. A review of single aerosol particle studies in the atmosphere of East Asia: morphology, mixing state, source, and heterogeneous reactions. J. Clean. Prod. 112, 1330–1349. http://dx.doi.org/10.1016/j.jclepro.2015.04.050.
Li, K., Chen, L., Han, K., Lv, B., Bao, K., Wu, X., Gao, X., Cen, K., 2017. Smog chamber study on aging of combustion soot in isoprene/SO2/NOx system: changes of mass, size, effective density, morphology and mixing state. Atmos. Res. 184, 139–148. http://dx.doi.org/10.1016/j.atmosres.2016.10.011.
Liu, D., Flynn, M., Gysel, M., Targino, A., Crawford, I., Bower, K., Choularton, T., Jurányi, Z., Steinbacher, M., Hüglin, C., Curtius, J., Kampus, M., Petzold, A., Weingartner, E., Baltensperger, U., Coe, H., 2010. Single particle characterization of black carbon aerosols at a tropospheric alpine site in Switzerland. Atmos. Chem. Phys. 10, 7389–7407. http://dx.doi.org/10.5194/acp-10-7389-2010.
Liu, D., Allan, J., Whitehead, J., Young, D., Flynn, M., Coe, H., McFiggans, G., Fleming, Z.L., Bandy, B., 2013. Ambient black carbon particle hygroscopic properties controlled by mixing state and composition. Atmos. Chem. Phys. 13, 2015–2029. http://dx.doi.org/10.5194/acp-13-2015-2013.
Liu, S., Aiken, A.C., Gorkowski, K., Dubey, M.K., Cappa, C.D., Williams, L.R., Herndon, S.C., Massoli, P., Fortner, E.C., Chhabra, P.S., Brooks, W.A., Onasch, T.B., Jayne, J.T., Worsnop, D.R., China, S., Sharma, N., Mazzoleni, C., Xu, L., Ng, N.L., Liu, D., Allan, J.D., Lee, J.D., Fleming, Z.L., Mohr, C., Zotter, P., Szidat, S., Prévôt, A.S.H., 2015. Enhanced light absorption by mixed source black and brown carbon particles in UK winter. Nat. Commun. 6, 8435. http://dx.doi.org/10.1038/ncomms9435.
Lobert, J.M., Scharffe, D.H., Hao, W.M., Crutzen, P.J., 1990. Importance of biomass burning in the atmospheric budgets of nitrogen-containing gases. Nature 346, 552–554. http://dx.doi.org/10.1038/346552a0.
McMeeking, G.R., Good, N., Petters, M.D., McFiggans, G., Coe, H., 2011a. Influences on the fraction of hydrophobic and hydrophilic black carbon in the atmosphere. Atmos. Chem. Phys. 11, 5099–5112. http://dx.doi.org/10.5194/acp-11-5099-2011.
McMeeking, G.R., Morgan, W.T., Flynn, M., Highwood, E.J., Turnbull, K., Haywood, J., Coe, H., 2011b. Black carbon aerosol mixing state, organic aerosols and aerosol optical properties over the United Kingdom. Atmos. Chem. Phys. 11, 9037–9052. http://dx.doi.org/10.5194/acp-11-9037-2011.
Metcalf, A.R., Craven, J.S., Ensberg, J.J., Brioude, J., Angevine, W., Sorooshian, A., Duong, H.T., Jonsson, H.H., Flagan, R.C., Seinfeld, J.H., 2012. Black carbon aerosol over the Los Angeles Basin during CalNex. J. Geophys. Res. Atmos. 117, D00V13. http://dx.doi.org/10.1029/2011JD017255.
Middlebrook, A.M., Bahreini, R., Jimenez, J.L., Canagaratna, M.R., 2012. Evaluation of composition-dependent collection efficiencies for the aerodyne aerosol mass spectrometer using field data. Aerosol Sci. Technol. 46, 258–271. http://dx.doi.org/10.1080/02786826.2011.620041.
Moffet, R.C., O'Brien, R.E., Alpert, P.A., Kelly, S.T., Pham, D.Q., Gilles, M.K., Knopf, D.A., Laskin, A., 2016. Morphology and mixing of black carbon particles collected in central California during the CARES field study. Atmos. Chem. Phys. 16, 14515–14525. http://dx.doi.org/10.5194/acp-16-14515-2016.
Moteki, N., Kondo, Y., 2007. Effects of mixing state on black carbon measurements by laser-induced incandescence. Aerosol Sci. Technol. 41, 398–417. http://dx.doi.org/10.1080/02786820701199728.
Moteki, N., Kondo, Y., 2010. Dependence of laser-induced incandescence on physical properties of black carbon aerosols: measurements and theoretical interpretation. Aerosol Sci. Technol. 44, 663–675. http://dx.doi.org/10.1080/02786826.2010.484450.
Moteki, N., Kondo, Y., Miyazaki, Y., Takegawa, N., Komazaki, Y., Kurata, G., Shirai, T., Blake, D.R., Miyakawa, T., Koike, M., 2007. Evolution of mixing state of black carbon particles: aircraft measurements over the western Pacific in March 2004. Geophys. Res. Lett. 34, L11803. http://dx.doi.org/10.1029/2006GL028943.
Nair, V.S., Moorthy, K.K., Alappattu, D.P., Kunhikrishnan, P.K., George, S., Nair, P.R., Babu, S.S., Abish, B., Satheesh, S.K., Tripathi, S.N., Niranjan, K., Madhavan, B.L., Srikant, V., Dutt, C.B.S., Badarinath, K.V.S., Reddy, R.R., 2007. Wintertime aerosol characteristics over the Indo-Gangetic Plain (IGP): impacts of local boundary layer processes and long-range transport. J. Geophys. Res. Atmos. 112, D13205. http://dx.doi.org/10.1029/2006JD008099.
Nakayama, T., Ikeda, Y., Sawada, Y., Setoguchi, Y., Ogawa, S., Kawana, K., Mochida, M., Ikemori, F., Matsumoto, K., Matsumi, Y., 2014. Properties of light-absorbing aerosols in the Nagoya urban area, Japan, in August 2011 and January 2012: contributions of brown carbon and lensing effect. J. Geophys. Res. Atmos. 119, 12721–12739. http://dx.doi.org/10.1002/2014JD021744.
Nakayama, T., Suzuki, H., Kagamitani, S., Ikeda, Y., Uchiyama, A., Matsumi, Y., 2015. Characterization of a three wavelength photoacoustic soot spectrometer (PASS-3) and a photoacoustic extinctiometer (PAX). J. Meteorol. Soc. Japan. Ser. II 93, 285–308. http://dx.doi.org/10.2151/jmsj.2015-016.
Novakov, T., Andreae, M.O., Gabriel, R., Kirchstetter, T.W., Mayol-Bracero, O.L., Ramanathan, V., 2000. Origin of carbonaceous aerosols over the tropical Indian Ocean: biomass burning or fossil fuels? Geophys. Res. Lett. 27, 4061–4064. http://dx.doi.org/10.1029/2000GL011759.
Oshima, N., Koike, M., Zhang, Y., Kondo, Y., Moteki, N., Takegawa, N., Miyazaki, Y., 2009. Aging of black carbon in outflow from anthropogenic sources using a mixing state resolved model: model development and evaluation. J. Geophys. Res. Atmos. 114, D06210. http://dx.doi.org/10.1029/2008JD010680.
Paatero, P., Tapper, U., 1994. Positive matrix factorization: a non-negative factor model with optimal utilization of error estimates of data values. Environmetrics 5, 111–126. http://dx.doi.org/10.1002/env.3170050203.
Peng, J., Hu, M., Guo, S., Du, Z., Zheng, J., Shang, D., Levy Zamora, M., Zeng, L., Shao, M., Wu, Y.-S., Zheng, J., Wang, Y., Glen, C.R., Collins, D.R., Molina, M.J., Zhang, R., 2016. Markedly enhanced absorption and direct radiative forcing of black carbon under polluted urban environments. Proc. Natl. Acad. Sci. 113, 4266–4271. http://dx.doi.org/10.1073/pnas.1602310113.
Penner, J.E., Chuang, C.C., Grant, K., 1998. Climate forcing by carbonaceous and sulfate aerosols. Clim. Dyn. 14, 839–851. http://dx.doi.org/10.1007/s003820050259.
Raju, M.P., Safai, P.D., Vijayakumar, K., Devara, P.C.S., Naidu, C.V., Rao, P.S.P., Pandithurai, G., 2016. Atmospheric abundances of black carbon aerosols and their radiative impact over an urban and a rural site in SW India. Atmos. Environ. 125, 429–436. http://dx.doi.org/10.1016/j.atmosenv.2015.09.023.
Ram, K., Sarin, M.M., 2015. Atmospheric carbonaceous aerosols from Indo-Gangetic Plain and Central Himalaya: impact of anthropogenic sources. J. Environ. Manag. 148, 153–163. http://dx.doi.org/10.1016/j.jenvman.2014.08.015.
Ram, K., Sarin, M.M., Tripathi, S.N., 2010. A 1 year record of carbonaceous aerosols from an urban site in the Indo-Gangetic Plain: characterization, sources, and temporal variability. J. Geophys. Res. 115, D24313. http://dx.doi.org/10.1029/2010JD014188.
Ram, K., Sarin, M.M., Sudheer, A.K., Rengarajan, R., 2012a. Carbonaceous and secondary inorganic aerosols during wintertime fog and haze over urban sites in the Indo-Gangetic plain. Aerosol Air Qual. Res. 12, 355–366. http://dx.doi.org/10.4209/aaqr.2011.07.0105.
Ram, K., Sarin, M.M., Tripathi, S.N., 2012b. Temporal trends in atmospheric PM 2.5, PM 10, elemental carbon, organic carbon, water-soluble organic carbon, and optical properties: impact of biomass burning emissions in the Indo-Gangetic Plain. Environ. Sci. Technol. 46, 686–695. http://dx.doi.org/10.1021/es202857w.

Ram, K., Tripathi, S.N., Sarin, M.M., Bhattu, D., 2014. Primary and secondary aerosols from an urban site (Kanpur) in the Indo-Gangetic Plain: impact on CCN, CN concentrations and optical properties. Atmos. Environ. 89, 655–663. http://dx.doi.org/10.1016/j.atmosenv.2014.02.009.

Ram, K., Singh, S., Sarin, M.M., Srivastava, A.K., Tripathi, S.N., 2016. Variability in aerosol optical properties over an urban site, Kanpur, in the Indo-Gangetic Plain: a case study of haze and dust events. Atmos. Res. 174–175, 52–61. http://dx.doi.org/10.1016/j.atmosres.2016.01.014.

Ramachandran, S., Rajesh, T.A., 2007. Black carbon aerosol mass concentrations over Ahmedabad, an urban location in western India: comparison with urban sites in Asia, Europe, Canada, and the United States. J. Geophys. Res. 112, D06211. http://dx.doi.org/10.1029/2006JD007488.

Ramanathan, V., Crutzen, P.J., Kiehl, J.T., Rosenfeld, D., 2001. Aerosols, climate, and the hydrological cycle. Science 294, 2119–2124. http://dx.doi.org/10.1126/science.1064034.

Saathoff, H., Naumann, K.H., Schnaiter, M., Schöck, W., Möhler, O., Schurath, U., Weingartner, E., Gysel, M., Baltensperger, U., 2003. Coating of soot and $(NH_4)_2SO_4$ particles by ozonolysis products of α-pinene. J. Aerosol Sci. 34, 1297–1321. http://dx.doi.org/10.1016/S0021-8502(03)00364-1.

Sanap, S.D., Pandithurai, G., 2015. The effect of absorbing aerosols on Indian monsoon circulation and rainfall: a review. Atmos. Res. 164–165, 318–327. http://dx.doi.org/10.1016/j.atmosres.2015.06.002.

Schwarz, J.P., Gao, R.S., Fahey, D.W., Thomson, D.S., Watts, L.A., Wilson, J.C., Reeves, J.M., Darbeheshti, M., Baumgardner, D.G., Kok, G.L., Chung, S.H., Schulz, M., Hendricks, J., Lauer, A., Kärcher, B., Slowik, J.G., Rosenlof, K.H., Thompson, T.L., Langford, A.O., Loewenstein, M., Aikin, K.C., 2006. Single-particle measurements of midlatitude black carbon and light-scattering aerosols from the boundary layer to the lower stratosphere. J. Geophys. Res. 111, D16207. http://dx.doi.org/10.1029/2006JD007076.

Schwarz, J.P., Gao, R.S., Spackman, J.R., Watts, L.A., Thomson, D.S., Fahey, D.W., Ryerson, T.B., Peischl, J., Holloway, J.S., Trainer, M., Frost, G.J., Baynard, T., Lack, D.A., de Gouw, J.A., Warneke, C., Del Negro, L.A., 2008. Measurement of the mixing state, mass, and optical size of individual black carbon particles in urban and biomass burning emissions. Geophys. Res. Lett. 35, L13810. http://dx.doi.org/10.1029/2008GL033968.

Schwarz, J.P., Spackman, J.R., Gao, R.S., Perring, A.E., Cross, E., Onasch, T.B., Ahern, A., Wrobel, W., Davidovits, P., Olfert, J., Dubey, M.K., Mazzoleni, C., Fahey, D.W., 2010. The detection efficiency of the Single Particle Soot Photometer. Aerosol Sci. Technol. 44, 612–628. http://dx.doi.org/10.1080/02786826.2010.481298.

Sedlacek, A.J., Lewis, E.R., Kleinman, L., Xu, J., Zhang, Q., 2012. Determination of and evidence for non-core-shell structure of particles containing black carbon using the Single-Particle Soot Photometer (SP2). Geophys. Res. Lett. 39, L06802. http://dx.doi.org/10.1029/2012GL050905.

Sedlacek, A.J., Lewis, E.R., Onasch, T.B., Lambe, A.T., Davidovits, P., 2015. Investigation of refractory black carbon-containing particle morphologies using the single-particle soot photometer (SP2). Aerosol Sci. Technol. 49, 872–885. http://dx.doi.org/10.1080/02786826.2015.1074978.

Shamjad, P.M., Tripathi, S.N., Aggarwal, S.G., Mishra, S.K., Joshi, M., Khan, A., Sapra, B.K., Ram, K., 2012. Comparison of experimental and modeled absorption enhancement by black carbon (BC) cored polydisperse aerosols under hygroscopic conditions. Environ. Sci. Technol. 46, 8082–8089. http://dx.doi.org/10.1021/es300295v.

Shamjad, P.M., Tripathi, S.N., Pathak, R., Hallquist, M., Arola, A., Bergin, M.H., 2015. Contribution of Brown carbon to direct radiative forcing over the Indo-Gangetic Plain. Environ. Sci. Technol. 49, 10474–10481. http://dx.doi.org/10.1021/acs.est.5b03368.

Shamjad, P.M., Tripathi, S.N., Thamban, N.M., Vreeland, H., 2016. Refractive index and absorption attribution of highly absorbing brown carbon aerosols from an urban Indian City-Kanpur. Sci Rep 6, 37735. http://dx.doi.org/10.1038/srep37735.

Shiraiwa, M., Kondo, Y., Moteki, N., Takegawa, N., Miyazaki, Y., Blake, D.R., 2007. Evolution of mixing state of black carbon in polluted air from Tokyo. Geophys. Res. Lett. 34, L16803. http://dx.doi.org/10.1029/2007GL029819.

Singh, R.P., Dey, S., Tripathi, S.N., Tare, V., Holben, B., 2004. Variability of aerosol parameters over Kanpur, northern India. J. Geophys. Res. Atmos. 109, D23206. http://dx.doi.org/10.1029/2004JD004966.

Singh, S., Tiwari, S., Gond, D.P., Dumka, U.C., Bisht, D.S., Tiwari, S., Pandithurai, G., Sinha, A., 2015. Intra-seasonal variability of black carbon aerosols over a coal field area at Dhanbad, India. Atmos. Res. 161–162, 25–35. http://dx.doi.org/10.1016/j.atmosres.2015.03.015.

Slowik, J.G., Cross, E.S., Han, J.-H., Davidovits, P., Onasch, T.B., Jayne, J.T., Williams, L.R., Canagaratna, M.R., Worsnop, D.R., Chakrabarty, R.K., Moosmüller, H., Arnott, W.P., Schwarz, J.P., Gao, R.-S., Fahey, D.W., Kok, G.L., Petzold, A., 2007. An intercomparison of instruments measuring black carbon content of soot particles. Aerosol Sci. Technol. 41, 295–314. http://dx.doi.org/10.1080/02786820701197078.

Stephens, M., Turner, N., Sandberg, J., 2003. Particle identification by laser-induced incandescence in a solid-state laser cavity. Appl. Opt. 42, 3726. http://dx.doi.org/10.1364/AO.42.003726.

Subramanian, R., Kok, G.L., Baumgardner, D., Clarke, A., Shinozuka, Y., Campos, T.L., Heizer, C.G., Stephens, B.B., de Foy, B., Voss, P.B., Zaveri, R.A., 2010. Black carbon over Mexico: the effect of atmospheric transport on mixing state, mass absorption cross-section, and BC/CO ratios. Atmos. Chem. Phys. 10, 219–237. http://dx.doi.org/10.5194/acp-10-219-2010.

Talukdar, S., Jana, S., Maitra, A., Gogoi, M.M., 2015. Characteristics of black carbon concentration at a metropolitan city located near land-ocean boundary in Eastern India. Atmos. Res. 153, 526–534. http://dx.doi.org/10.1016/j.atmosres.2014.10.014.

Tiwari, S., Dumka, U.C., Hopke, P.K., Tunved, P., Srivastava, A.K., Bisht, D.S., Chakrabarty, R.K., 2016. Atmospheric heating due to black carbon aerosol during the summer monsoon period over Ballia: a rural environment over Indo-Gangetic Plain. Atmos. Res. 178–179, 393–400. http://dx.doi.org/10.1016/j.atmosres.2016.04.008.

Tripathi, S.N., Dey, S., Tare, V., Satheesh, S.K., 2005a. Aerosol black carbon radiative forcing at an industrial city in northern India. Geophys. Res. Lett. 32, 1–4. http://dx.doi.org/10.1029/2005GL022515.

Tripathi, S.N., Dey, S., Tare, V., Satheesh, S.K., Lal, S., Venkataramani, S., 2005b. Enhanced layer of black carbon in a north Indian industrial city. Geophys. Res. Lett. 32, L08802. http://dx.doi.org/10.1029/2005GL022564.

Tripathi, S.N., Srivastava, A.K., Dey, S., Satheesh, S.K., Krishnamoorthy, K., 2007. The vertical profile of atmospheric heating rate of black carbon aerosols at Kanpur in northern India. Atmos. Environ. 41, 6909–6915. http://dx.doi.org/10.1016/j.atmosenv.2007.06.032.

Ueda, S., Nakayama, T., Taketani, F., Adachi, K., Matsuki, A., Iwamoto, Y., Sadanaga, Y., Matsumi, Y., 2016. Light absorption and morphological properties of soot-containing aerosols observed at an East Asian outflow site, Noto Peninsula, Japan. Atmos. Chem. Phys. 16, 2525–2541. http://dx.doi.org/10.5194/acp-16-2525-2016.

Vaishya, A., Singh, P., Rastogi, S., Babu, S.S., 2017. Aerosol black carbon quantification in the central Indo-Gangetic Plain: seasonal heterogeneity and source apportionment. Atmos. Res. 185, 13–21. http://dx.doi.org/10.1016/j.atmosres.2016.10.001.

Verma, S., Reddy, D.M., Ghosh, S., Kumar, D.B., Chowdhury, A.K., 2017. Estimates of spatially and temporally resolved constrained black carbon emission over the Indian region using a strategic integrated modelling approach. Atmos. Res. 195, 9–19. http://dx.doi.org/10.1016/j.atmosres.2017.05.007.

Wang, Q., Huang, R.-J., Cao, J., Han, Y., Wang, G., Li, G., Wang, Y., Dai, W., Zhang, R., Zhou, Y., 2014a. Mixing state of black carbon aerosol in a heavily polluted urban area of China: implications for light absorption enhancement. Aerosol Sci. Technol. 48, 689–697. http://dx.doi.org/10.1080/02786826.2014.917758.

Wang, Q., Schwarz, J.P., Cao, J., Gao, R., Fahey, D.W., Hu, T., Huang, R.J., Han, Y., Shen, Z., 2014b. Black carbon aerosol characterization in a remote area of Qinghai-Tibetan Plateau, western China. Sci. Total Environ. 479–480, 151–158. http://dx.doi.org/10.1016/j.scitotenv.2014.01.098.

Wang, Q.Y., Huang, R.-J., Cao, J.J., Tie, X.X., Ni, H.Y., Zhou, Y.Q., Han, Y.M., Hu, T.F., Zhu, C.S., Feng, T., Li, N., Li, J.D., 2015. Black carbon aerosol in winter northeastern Qinghai–Tibetan Plateau, China: the source, mixing state and optical property. Atmos. Chem. Phys. 15, 13059–13069. http://dx.doi.org/10.5194/acp-15-13059-2015.

Wang, Q., Huang, R.-J., Zhao, Z., Zhang, N., Wang, Y., Ni, H., Tie, X., Han, Y., Zhuang, M., Wang, M., Zhang, J., Zhang, X., Dusek, U., Cao, J., 2016. Size distribution and mixing state of refractory black carbon aerosol from a coastal city in South China. Atmos. Res. 181, 163–171. http://dx.doi.org/10.1016/j.atmosres.2016.06.022.

Weingartner, E., Burtscher, H., Baltensperger, U., 1997. Hygroscopic properties of carbon and diesel soot particles. Atmos. Environ. 31, 2311–2327. http://dx.doi.org/10.1016/S1352-2310(97)00023-X.

Willis, M.D., Healy, R.M., Riemer, N., West, M., Wang, J.M., Jeong, C.-H., Wenger, J.C., Evans, G.J., Abbatt, J.P.D., Lee, A.K.Y., 2016. Quantification of black carbon mixing state from traffic: implications for aerosol optical properties. Atmos. Chem. Phys. 16, 4693–4706. http://dx.doi.org/10.5194/acp-16-4693-2016.

Zhang, R., Khalizov, A.F., Pagels, J., Zhang, D., Xue, H., McMurry, P.H., 2008. Variability in morphology, hygroscopicity, and optical properties of soot aerosols during atmospheric processing. Proc. Natl. Acad. Sci. U. S. A. 105, 10291–10296. http://dx.doi.org/10.1073/pnas.0804860105.

Zhang, G., Han, B., Bi, X., Dai, S., Huang, W., Chen, D., Wang, X., Sheng, G., Fu, J., Zhou, Z., 2015. Characteristics of individual particles in the atmosphere of Guangzhou by single particle mass spectrometry. Atmos. Res. 153, 286–295. http://dx.doi.org/10.1016/j.atmosres.2014.08.016.

Zhang, Y., Zhang, Q., Cheng, Y., Su, H., Kecorius, S., Wang, Z., Wu, Z., Hu, M., Zhu, T., Wiedensohler, A., He, K., 2016. Measuring the morphology and density of internally mixed black carbon with SP2 and VTDMA: new insight into the absorption enhancement of black carbon in the atmosphere. Atmos. Meas. Tech. 9, 1833–1843. http://dx.doi.org/10.5194/amt-9-1833-2016.